INTERNATIONAL JOURNAL FOR NUMERICAL METHODS IN ENGINEERING
Int. J. Numer. Meth. Engng 2017; **00**:1–41 *Prepared using* nmeauth.cls *[Version: 2002/09/18 v2.02]*

Explicit Multistep Time Integration for Discontinuous Elastic Stress Wave Propagation in Heterogeneous Solids

S. S. Cho[1], R. Kolman[2], José A. González[3] and K. C. Park[4,*]

[1]*RAM Transportation and Storage Technology Division, Korea Atomic Energy Research Institute, 111 Daedeok-daero 989beon-gil, Yuseong-gu, Daejeon 34057, Korea*
[2]*Institute of Thermomechanics, The Czech Academy of Sciences, Dolejškova 5, 182 00 Prague, Czech Republic*
[3]*Escuela Téchica Superior de Ingeniería, Universidad de Sevilla, Camino de los Descubrimientos s/n, Seville E-41902, Spain*
[4]*Department of Aerospace Engineering Sciences, University of Colorado, Boulder, CO 80309-429, USA*

SUMMARY

A multistep explicit time integration algorithm is presented for tracking the propagation of discontinuous stress waves in heterogeneous solids whose subdomain to subdomain critical time step ratios range from tens to thousands. The present multistep algorithm offers efficient as well as accurate computations for tracking discontinuous waves propagating through such heterogeneous solids. The present algorithm, first, employs the partitioned formulation for representing each subdomain, whose interface compatibility is enforced via the method of the localized Lagrange multipliers. Second, for each subdomain, the governing equations of motion are decomposed into the extensional and shear components so that tracking of waves of different propagation speeds are treated with different critical step sizes to significantly reduce the computational dispersion errors. Accuracy of the present algorithm is demonstrated as applied to the stress wave propagation in one dimenstional heterogeneous bar and in heterogeneous plain stress problems. Copyright © 2017 John Wiley & Sons, Ltd.

KEY WORDS: explicit multistep time integration; heterogeneous solids; localized Lagrange multipliers; Component-wise partitioned equations of motion

1. Introduction

Recently, as the performance of the mechanical technology has been improved, various kinds of materials have been used in the machine, and as the operation speed has increased, it has become a necessary requirement to design the machine so as to perform its functions while being subjected to an impact load. Therefore, the study on the impact problem of a machine made of different materials is recognized as an important issue not only in the safety design of the machine but also in the overall machine industry. Since the deformation behavior of the dissimilar materials subjected to the impact

*Correspondence to: K.C. Park, Department of Aerospace Engineering Sciences, University of Colorado, Boulder, CO 80309-429, USA. E-mail: kcpark@colorado.edu

Received 15 June 2017
Revised

load is determined by the transmission and reflection of the stress wave at the their own interfaces, it is necessary to study the propagation of the stress wave at the interface of the heterogeneous materials. Currently, the propagation of the stress wave on a single material and the dispersion and dissipation error due to numerical analysis have been studied extensively. However, there are very few researches on the propagation of stress wave on heterogeneous materials. The study of stress waves began in the mid-nineteenth century, and Kolsky conducted a limited study on simple one-dimensional or two-dimensional problems, although the theory of propagation of stress waves in elastodynamics was first systematized[1]. Since the governing equation of this wave propagation is represented by the hyperbolic equation, the definition of the stress wave has discontinuity or singularity at the wave front. Therefore, theoretical approaches to the propagation of stress waves by the computation of the stress fields in complex solids have been limited, and many researchers have been actively studying the methods of solving the hyperbolic equations using the finite element method[2]. Reed and Hill drastically reduced the numerical dispersion error by introducing a discontinuous Galerkin method for the calculation of the neutron transport equation consisting of hyperbolic equations[3]. Hughes et al. proposed a finite element method using a space-time discontinuous Galerkin method to analyze the propagation of stress wave in a solid body, and conducted a study on convergence and stability[4, 5, 6]. Marsden et al. numerically integrated the equations governing the mechanical system by taking the variational principle in the action integral of the discrete Hamiltonian rather than the equations of motion[7, 8]. Cho et al. proposed a method to reduce dispersion error and dissipation error of stress wave by introducing a discontinuity operator in the variational integrator[9].

Numerical analysis of transmission and reflection of stress waves in heterogeneous solids was done by a few researchers. Prager describes mathematically the continuous conditions of displacement and stress at the discontinuous interface in the linear elastic problem as a classical principle of variational method and describes how to apply to the finite element method[10]. Virieux proposed the velocity-stress finite difference method to numerically calculate the P-SV and SH wave propagation problems in heterogeneous media in the viewpoint of seismologists[11, 12]. Park et al. proposed the new integration formula that is obtained by push-forward-pullback operators in time element-by-element designed to filter post-shock oscillation, and the central difference method that intrinsically filters front-shock oscillations[13]. A judicious combination of these two characteristics has been shown to substantially reduce both spurious front-shock and post-shock oscillations in one-dimensional heterogeneous solids. For multidimensional solids, the component-wise partitioned equations of motions of extensional and shear stress components were developed, each of the decomposed equations of motion are integrated by the the push-forward-pullback operators[14]. As a result, the front-shock and post-shock spurious oscillations are shown to be significantly reduced and the wave fronts of different speeds were tailored to track by way of stiffness decomposition of the total stiffness into extension and shear components. Kolman et al. proposed an improving method for efficiently performing reference [14] and extended this method to impact problems with contact conditions[15]. Gravouil et al. proposed the multi-time-step with different time discretization in each subdomain which allows to couple explicit and implicit numerical methods[16, 17]. They also presented heterogeneous asynchronous time integrators(HATI) for computational structural dynamics which used an alternative dual approach based on the velocity continuity at the interface between heterogeneous time integrators[18].

This paper presents a multistep time integration algorithm for computing the discontinuous stress wave propagation in heterogeneous solids. The multistep time integration is able to be performed separately using their own critical time step sizes for the larger time step domain and the smaller time step domain. This study adopts the component-wise partitioned equations of motion and the push-forward pullback time integration in order to reduce the computational dispersion errors in

heterogeneous materials with significantly large time step ratios. The continuity of the interface between heterogeneous time integrators considers traction, acceleration, and velocity continuities, all of which are enforced via the method of localized Lagrange multipliers.

2. Governing Equations

This section briefly reviews the fundamental equation of motion for the dynamic problem and the corresponding component-wise partitioned equations of the longitudinal and shear stress waves in solids and the push-forward and pullback explicit time integration algorithm [14, 15, 19, 20].

2.1. Strong form of dynamic problem in solids

Let $(\Omega \subset \mathbb{R}^3)$ be an open and bounded domain with piecewise smooth boundary $\Gamma = \partial\Omega$. The strong formulation of dynamic problem in solid is written as,

$$\begin{aligned} \rho\ddot{u}_i &= \sigma_{ij,j} + b_i \; in \; \mathbf{\Omega} \times [t^0, T] \\ \sigma_{ij} &= C_{ijkl} u_{k,l} \\ u_i &= g_i \; on \; \mathbf{\Gamma}_{D_i} \times [t^0, T] \\ \sigma_{ij} n_j &= h_i \; on \; \mathbf{\Gamma}_{N_i} \times [t^0, T] \\ u_i(\mathbf{x}, t^0) &= u_i^0 \; for \; \mathbf{x} \in \mathbf{\Omega} \\ \dot{u}_i(\mathbf{x}, t^0) &= \dot{u}_i^0 \; for \; \mathbf{x} \in \mathbf{\Omega} \end{aligned} \tag{1}$$

where $b_i : \mathbf{\Omega} \times [t^0, T] \rightarrow \mathbb{R}$, $g_i : \mathbf{\Gamma}_{D_i} \times [t^0, T] \rightarrow \mathbb{R}$, $h_i : \mathbf{\Gamma}_{N_i} \times [t^0, T] \rightarrow \mathbb{R}$. In the aforesaid relationships, the superimposed dots denote the derivatives with respect to time. Equation (1) has a meaning of the equation of motion and σ_{ij} is the Cauchy stress tensor and C_{ijkl} is the 4th order tensor for the material constants. g_i and h_i prescribe the kinematic (Dirichlet type) boundary conditions and the traction (Neumann type) boundary conditions, respectively. u_i^0 and $\dot{u}_i^0$are the initial displacement and velocity. Furthermore, the piecewise smooth boundary is denotes $\Gamma = \overline{\mathbf{\Gamma}_{D_i} \cup \mathbf{\Gamma}_{N_i}}$and $\mathbf{\Gamma}_{D_i} \cap \mathbf{\Gamma}_{N_i} = \emptyset$.

2.2. Component-wise partitioned equations of motion in homogeneous solids

On the basis of the previous study[14], the total discrete displacement $(\mathbf{u})$ in element-by-element level can be decomposed into the discrete longitudinal and shear displacements $(\mathbf{u}_\sigma, \mathbf{u}_\tau)$ by the following formula:

$$\begin{aligned} \mathbf{u} &= \mathbf{u}_\sigma + \mathbf{u}_\tau \\ \mathbf{u}_\sigma &= \mathbf{D}_\sigma \mathbf{u} \\ \mathbf{u}_\tau &= \mathbf{D}_\tau \mathbf{u} \end{aligned} \tag{2}$$

where $(\mathbf{D}_\sigma, \mathbf{D}_\tau)$ are the component-wise partitioning operators for deriving the component-wise partitioned equations of motion. And the subscripts σ and τ mean the longitudinal and shear components, respectively. The virtual work for a generic element may be written as,

$$\delta\Pi(\mathbf{u}) = \delta\mathbf{u}^T = (\mathbf{f} - \mathbf{K}\mathbf{u} - \mathbf{M}\ddot{\mathbf{u}}) \tag{3}$$

Not only employing the element mass commutability, the element mass and the stiffness orthogonality relations, but also substituting Equations (2) into Equation (3), the virtual work can be decomposed into the following partitioned virtual work[14, 15]:

$$\delta\Pi(\mathbf{u}_\sigma, \mathbf{u}_\tau) = \delta\mathbf{u}_\sigma^T(\mathbf{f}_\sigma - \mathbf{K}_\sigma\mathbf{u}_\sigma - \mathbf{M}_\sigma\ddot{\mathbf{u}}_\sigma) + \delta\mathbf{u}_\tau^T(\mathbf{f}_\tau - \mathbf{K}_\tau\mathbf{u}_\tau - \mathbf{M}_\tau\ddot{\mathbf{u}}_\tau) \tag{4}$$

where

$$\begin{aligned}
\mathbf{f} &= \mathbf{f}_\sigma + \mathbf{f}_\tau \\
\mathbf{K} &= \mathbf{K}_\sigma + \mathbf{K}_\tau \\
\mathbf{M} &= \mathbf{M}_\sigma + \mathbf{M}_\tau \\
\mathbf{f}_\sigma &= \mathbf{D}_\sigma^T\mathbf{f} \\
\mathbf{f}_\tau &= \mathbf{D}_\tau^T\mathbf{f} \\
\mathbf{K}_\sigma &= \mathbf{D}_\sigma^T\mathbf{K}\mathbf{D}_\sigma \\
\mathbf{K}_\tau &= \mathbf{D}_\tau^T\mathbf{K}\mathbf{D}_\tau \\
\mathbf{M}_\sigma &= \mathbf{D}_\sigma^T\mathbf{M}\mathbf{D}_\sigma \\
\mathbf{M}_\tau &= \mathbf{D}_\tau^T\mathbf{M}\mathbf{D}_\tau
\end{aligned} \tag{5}$$

Due to the orthgonality and commutability properties of the element mass and stiffness matrices, the virtual work equation (4) can eliminate the subscripts(σ and τ) in the component partitioned mass matrices($\mathbf{M}_\sigma$ and $\mathbf{M}_\tau$), and the component partitioned displacement fields($\mathbf{u}_\sigma$, $\mathbf{u}_\tau$) as shown in (6) [14, 15]. Therefore, we obtain the following element-by-element component-wise(modally) partitioned equations of motion as follows,

$$\begin{aligned}
\textit{Longitudinal component equation} &: \mathbf{M}\ddot{\mathbf{u}}_\sigma + \mathbf{K}_\sigma\mathbf{u} = \mathbf{f}_\sigma \\
\textit{Shear component equation} &: \mathbf{M}\ddot{\mathbf{u}}_\tau + \mathbf{K}_\tau\mathbf{u} = \mathbf{f}_\tau
\end{aligned} \tag{6}$$

And, the element total displacement $(\mathbf{u})$ needs to be related to the assembled global displacement $(\mathbf{w})$ via the following assembly operator:

$$\begin{aligned}
\mathbf{u} &= \mathbf{L}\mathbf{w} \\
\mathbf{w} &= (\mathbf{L}^T\mathbf{L})^{-1}\mathbf{L}^T\mathbf{u}
\end{aligned} \tag{7}$$

where $\mathbf{L}$ is the assembly Boolean matrix that is readily available in most finite element analysis codes.

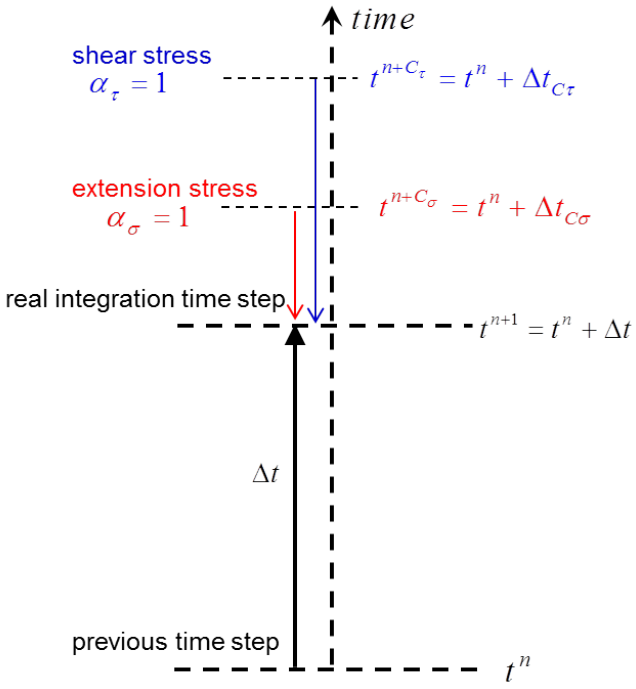

Figure 1. The relations between the three time steps in push-forward pullback time integration for component-wise partitioned equations of motion.

2.3. *Push-forward pullback time integration for component-wise partitioned equations of motion*

The explicit time integration algorithm for component-wise partitioned equations of motion has been proposed in [14, 15]. In this section, we briefly describe the algorithm for a general nonlinear dynamic problem in homogeneous solid, and Fig. 1 shows the relations between the three time steps for the proposed algorithm in multi-dimensional problem.

Step 1 : Assuming we have $(\mathbf{w}^n, \dot{\mathbf{w}}^n, \ddot{\mathbf{w}}^n)$ at time $t = t^n$, obtain the component-wise displacements at two critical time steps $(t^{n+C_\sigma} = t^n + \Delta t_{C_\sigma}, t^{n+C_\tau} = t^n + \Delta t_{C_\tau})$:

$$\begin{aligned} \mathbf{w}^{n+C_\sigma} &= \mathbf{w}^n + \Delta t_{C_\sigma} \dot{\mathbf{w}}^n + \frac{\Delta t_{C_\sigma}^2}{2} \ddot{\mathbf{w}}^n \\ \mathbf{w}^{n+C_\tau} &= \mathbf{w}^n + \Delta t_{C_\tau} \dot{\mathbf{w}}^n + \frac{\Delta t_{C_\tau}^2}{2} \ddot{\mathbf{w}}^n \end{aligned} \tag{8}$$

Step 2 : Compute the accelerations at two critical time steps(longitudinal and shear components):

$$\begin{aligned} \ddot{\mathbf{u}}_\sigma^{n+C_\sigma} &= \mathbf{M}^{-1}(\mathbf{f}_\sigma^{n+C_\sigma} - \mathbf{K}_\sigma \mathbf{u}^{n+C_\sigma}) \\ \ddot{\mathbf{u}}_\tau^{n+C_\tau} &= \mathbf{M}^{-1}(\mathbf{f}_\tau^{n+C_\tau} - \mathbf{K}_\tau \mathbf{u}^{n+C_\tau}) \end{aligned} \tag{9}$$

Step 3 : Perform the pushforward pullback time integration with a parameter $\theta \in [0, 1]$ ($\theta = 1/2$

for the averaged displacement of the pushforward and pullback time integrations, $\theta = 0$ for the conventional central difference method):

$$\begin{aligned}\mathbf{u}^{n+1} = \mathbf{u}^n + \Delta t\dot{\mathbf{u}}^n + \beta_{1\sigma}(\Delta t_{C_\sigma})^2\ddot{\mathbf{u}}_\sigma^n + \beta_{2\sigma}(\Delta t_{C_\sigma})^2\ddot{\mathbf{u}}_\sigma^{n+C_\sigma} \\ +\beta_{1\tau}(\Delta t_{C_\tau})^2\ddot{\mathbf{u}}_\tau^n + \beta_{2\tau}(\Delta t_{C_\tau})^2\ddot{\mathbf{u}}_\tau^{n+C_\tau} \\ \ddot{\mathbf{u}}^{n+1} = \mathbf{M}^{-1}(\mathbf{f} - \mathbf{K}\mathbf{u}^{n+1}) \\ \dot{\mathbf{u}}^{n+1} = \dot{\mathbf{u}}^n + \Delta t\{(1-\gamma)\ddot{\mathbf{u}}^n + \gamma\ddot{\mathbf{u}}^{n+1}\}\end{aligned} \tag{10}$$

where,

$$\begin{aligned}\alpha_\sigma = \Delta t/\Delta t_{C_\sigma},\ \alpha_\tau = \Delta t/\Delta t_{C_\tau} \\ \beta_{1\sigma} = \frac{\alpha_\sigma}{6}(3\alpha_\sigma + \theta - \theta\alpha_\sigma^2),\ \beta_{2\sigma} = \frac{\theta\alpha_\sigma}{6}(\alpha_\sigma^2 - 1) \\ \beta_{1\tau} = \frac{\alpha_\tau}{6}(3\alpha_\tau + \theta - \theta\alpha_\tau^2),\ \beta_{2\tau} = \frac{\theta\alpha_\tau}{6}(\alpha_\tau^2 - 1) \\ Stability\ condition : \Delta t \le \Delta t_{C_\sigma}\end{aligned} \tag{11}$$

Step 4 : Decompose the acceleration $\ddot{\mathbf{u}}^{n+1}$ to longitudinal and shear components $\ddot{\mathbf{u}}_\sigma^{n+1}$ and $\ddot{\mathbf{u}}_\tau^{n+1}$.

$$\ddot{\mathbf{u}}^{n+1} = \ddot{\mathbf{u}}_\sigma^{n+1} + \ddot{\mathbf{u}}_\tau^{n+1} \tag{12}$$

Step 5 : Obtain the assembled displacement, velocity and acceleration:

$$\begin{aligned}\mathbf{w}^{n+1} = (\mathbf{L}^T\mathbf{L})^{-1}\mathbf{L}^T\mathbf{u}^{n+1} \\ \dot{\mathbf{w}}^{n+1} = (\mathbf{L}^T\mathbf{L})^{-1}\mathbf{L}^T\dot{\mathbf{u}}^{n+1} \\ \ddot{\mathbf{w}}^{n+1} = (\mathbf{L}^T\mathbf{L})^{-1}\mathbf{L}^T\ddot{\mathbf{u}}^{n+1}\end{aligned} \tag{13}$$

3. **Partitioned explicit-explicit integration for two dimensional problem**

Fig. 2 shows two domains for two-dimensional heterogeneous problem. L-domain means a region with a larger time step, and S-domain is a region with a smaller time step. Γ_I is the interface boundary between the heterogeneous domains, and $\mathbf{u}_f$ denote the global displacement corresponding to the frame nodes in Γ_I, Two localized Lagrange multipliers, $\boldsymbol{\lambda}_L$ and $\boldsymbol{\lambda}_S$, are the interface loads at the corresponding frame nodes between two domains. Before reading the present algorithm for two dimensional problem, we strongly suggest reading the appendix for one dimensional algorhtm at the back of this paper.

The equations of motion in two heterogeneous domains can be written as,

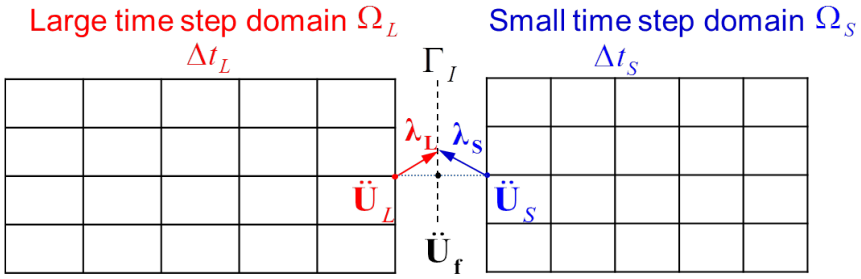

Figure 2. Two dimensional heterogeneous solids including L-domain and S-domain.

Component-wise partitioned equations of motion

(1) Extensional components

$$\begin{aligned}\mathbf{M}_L\ddot{\mathbf{u}}_{L\sigma} + \mathbf{K}_{L\sigma}\mathbf{u}_L &= \mathbf{D}_\sigma^T(\mathbf{f}_L - \mathbf{B}_L\boldsymbol{\lambda}_L)\ in\ \boldsymbol{\Omega}_L \\ \mathbf{M}_S\ddot{\mathbf{u}}_{S\sigma} + \mathbf{K}_{S\sigma}\mathbf{u}_S &= \mathbf{D}_\sigma^T(\mathbf{f}_S - \mathbf{B}_S\boldsymbol{\lambda}_S)\ in\ \boldsymbol{\Omega}_S\end{aligned} \tag{14}$$

(2) Shear components

$$\begin{aligned}\mathbf{M}_L\ddot{\mathbf{u}}_{L\tau} + \mathbf{K}_{L\tau}\mathbf{u}_L &= \mathbf{D}_\tau^T(\mathbf{f}_L - \mathbf{B}_L\boldsymbol{\lambda}_L)\ in\ \boldsymbol{\Omega}_L \\ \mathbf{M}_S\ddot{\mathbf{u}}_{S\tau} + \mathbf{K}_{S\tau}\mathbf{u}_S &= \mathbf{D}_\tau^T(\mathbf{f}_S - \mathbf{B}_S\boldsymbol{\lambda}_S)\ in\ \boldsymbol{\Omega}_S\end{aligned} \tag{15}$$

The subscripts, L and S, designate the larger time step domain and the smaller time step domain, respectively. And $\mathbf{B}_L$ and $\mathbf{B}_S$ are the Boolean matrices that extracts the interface DOFs for each domains. The accelerations and the interface loads at the interface DOFs should be continuous kinematically and kinetically as follows,

Kinematic Interface Continuities

$$\begin{aligned}\mathbf{B}_L^T\ddot{\mathbf{u}}_L - \mathbf{L}_L\ddot{\mathbf{u}}_f &= 0\ on\ \Gamma_I \\ \mathbf{B}_S^T\ddot{\mathbf{u}}_S - \mathbf{L}_S\ddot{\mathbf{u}}_f &= 0\ on\ \Gamma_I\end{aligned} \tag{16}$$

Traction Continuities

$$\mathbf{L}_L^T \boldsymbol{\lambda}_L + \mathbf{L}_S^T \boldsymbol{\lambda}_S = 0 \; on \; \Gamma_I \tag{17}$$

where $\ddot{\mathbf{u}}_f$ and $\mathbf{u}_f$ denote the global acceleration and displacement corresponding to the frame nodes. Γ_I is the interface boundary between two domains. $\mathbf{L}_L$ and $\mathbf{L}_S$ are the Boolean matrices that relates the interface DOFs to the global acceleration and displacement, and these are obtained by removing columns with all zero elements from $\mathbf{B}_L^T\mathbf{L}$ and $\mathbf{B}_S^T\mathbf{L}$, respectively.

The above three equations are continuity conditions for obtaining the Lagrange multipliers($\boldsymbol{\lambda}_L, \boldsymbol{\lambda}_S$ and $\mathbf{u}_f$) at the corresponding interface nodes in the current integration time step. However, when two solids are perfectly bonded in highly heterogeneous materials, there is a possiblitiy of 'drifting' that the displacement and velocity at the corresponding interface nodes of each material can differ during the actual time integration. Therefore, the following continuity conditions are simply applied to each integration step(t^{n+1}) of L-domain to prevent such the drifting phenomenon.

Kinematic continuities to prevent the drifting

$$\begin{aligned} \mathbf{B}_L^T \dot{\mathbf{u}}_L - \mathbf{L}_L \dot{\mathbf{u}}_f = \mathbf{B}_L^T \mathbf{u}_L - \mathbf{L}_L \mathbf{u}_f = 0 \; on \; \Gamma_I \\ \mathbf{B}_S^T \dot{\mathbf{u}}_S - \mathbf{L}_L \dot{\mathbf{u}}_f = \mathbf{B}_S^T \mathbf{u}_S - \mathbf{L}_S \mathbf{u}_f = 0 \; on \; \Gamma_I \end{aligned} \tag{18}$$

Unlike one dimensional problem, the time step and the critical time step for L-domain are defined as follows.

$$\begin{aligned} Time \; at \; L-domain : t^{n+1} = t^n + \Delta t_L^{n+1} \\ \Delta t_{CL}^{\sigma} = L_{min}^e / C_L^{\sigma} = Critical \; time \; step \; size \; for \; longitudinal \; component \\ \Delta t_{CL}^{\tau} = L_{min}^e / C_L^{\tau} = Critical \; time \; step \; size \; for \; shear \; component \\ Integration \; time \; step \; size \; in \; L-Domain : \Delta t_L^{n+1} = \Delta t_L \\ Ratio \; of \; two \; time \; step \; sizes \\ \alpha_L^{\sigma} = \Delta t_L / \Delta t_{CL}^{\sigma} \\ \alpha_L^{\tau} = \Delta t_L / \Delta t_{CL}^{\tau} \end{aligned} \tag{19}$$

where L_{min}^e means the minimum characteristic length of an element, and C_L^{σ} and C_L^{τ} are the propagation speed of longitudinal and shear stress in L-domain, respectively.

The time step in S-domain can be defined as shown in Equation (20) .

$$\begin{aligned} Time \; at \; S-domain : t^{n+j} = t^n + k\Delta t^{n+j} \\ \Delta t_{CS}^{\sigma} = L_{min}^e / C_S^{\sigma} = Critical \; time \; step \; size \; for \; longitudinal \; component \\ \Delta t_{CS}^{\tau} = L_{min}^e / C_S^{\tau} Critical \; time \; step \; size \; for \; shear \; component \\ Integration \; time \; step \; size \; in \; sub-step : \Delta t^{n+j} = \Delta t_S \\ Ratio \; of \; two \; time \; step \; sizes \\ \alpha_S^{\sigma} = \Delta t_S / \Delta t_{CS}^{\sigma} \\ \alpha_S^{\tau} = \Delta t_S / \Delta t_{CS}^{\tau} \end{aligned} \tag{20}$$

where C_S^σ and C_S^τ are the propagation speed of longitudinal and shear stress in S-domain, respectively.

And 'j' means the k-th integration sub-step in S-domain, and it is defined as,

$$j = \frac{k}{m} \; for \; k = 1, 2, \cdots, m$$
$$m = \Delta t_L / \Delta t_S \tag{21}$$

where 'k' is the oder of sub-step in S-domain during a time step in L-domain as same as one-dimensional problem(See Appendix for the details) and 'm' should be an integer. Therefore, we can describe the displacement and acceleration at k-th substep of S-domain during (n+1)th step of L-domain as shown in Equation (22).

All element on S-domain at $t^{n+j} = t^n + k\Delta t_S$

$$\begin{aligned}
\mathbf{u}_S^{n+j} &= \mathbf{u}_S^{n+j_o} + \Delta t_S \dot{\mathbf{u}}_S^{n+j_o} + \beta_{1S}^\sigma (\Delta t_{CS}^\sigma)^2 \ddot{\mathbf{u}}_{S\sigma}^{n+j_o} + \beta_{2S}^\sigma (\Delta t_{CS}^\sigma)^2 \ddot{\mathbf{u}}_{S\sigma}^{n+jC_S^\sigma} \\
&\quad + \beta_{1S}^\tau (\Delta t_{CS}^\tau)^2 \ddot{\mathbf{u}}_{S\tau}^{n+j_o} + \beta_{2S}^\tau (\Delta t_{CS}^\tau)^2 \ddot{\mathbf{u}}_{S\tau}^{n+jC_S^\tau} \\
\ddot{\mathbf{u}}_S^{n+j} &= \mathbf{M}_S^{-1} \left(\mathbf{f}_S - \mathbf{K}_S \mathbf{u}_S^{n+j} \right) - \mathbf{M}_S^{-1} \mathbf{B}_S \boldsymbol{\lambda}_S^{n+j} = \tilde{\ddot{\mathbf{u}}}_S^{n+j} - \mathbf{M}_S^{-1} \mathbf{B}_S \boldsymbol{\lambda}_S^{n+j} \\
\ddot{\mathbf{u}}_{S\sigma}^{n+jC_S^\sigma} &= \tilde{\ddot{\mathbf{u}}}_S^{n+jC_S^\sigma} - \mathbf{M}_S^{-1} \mathbf{D}_\sigma^T \mathbf{B}_S \boldsymbol{\lambda}_S^{n+jC_S^\sigma} \\
\ddot{\mathbf{u}}_{S\tau}^{n+jC_S^\tau} &= \tilde{\ddot{\mathbf{u}}}_S^{n+jC_S^\tau} - \mathbf{M}_S^{-1} \mathbf{D}_\tau^T \mathbf{B}_S \boldsymbol{\lambda}_S^{n+jC_S^\tau} \\
\mathbf{u}_S^{n+jC_S^\sigma} &= \mathbf{u}_S^{n+j_o} + \Delta t_{CS}^\sigma \dot{\mathbf{u}}_S^{n+j_o} + \frac{1}{2} (\Delta t_{CS}^\sigma)^2 \ddot{\mathbf{u}}_S^{n+j_o} \\
\mathbf{u}_S^{n+jC_S^\tau} &= \mathbf{u}_S^{n+j_o} + \Delta t_{CS}^\tau \dot{\mathbf{u}}_S^{n+j_o} + \frac{1}{2} (\Delta t_{CS}^\tau)^2 \ddot{\mathbf{u}}_S^{n+j_o} \\
\tilde{\ddot{\mathbf{u}}}_S^{n+j} &= \mathbf{M}_S^{-1} \left(\mathbf{f}_S^{n+j} - \mathbf{K}_S \mathbf{u}_S^{n+j} \right) \\
\tilde{\ddot{\mathbf{u}}}_S^{n+jC_S^\sigma} &= \mathbf{M}_S^{-1} \left(\mathbf{f}_S^{n+jC_S^\sigma} - \mathbf{K}_S \mathbf{u}_S^{n+jC_S^\sigma} \right) \\
\tilde{\ddot{\mathbf{u}}}_S^{n+jC_S^\tau} &= \mathbf{M}_S^{-1} \left(\mathbf{f}_S^{n+jC_S^\tau} - \mathbf{K}_S \mathbf{u}_S^{n+jC_S^\tau} \right) \\
j_o &= \frac{k-1}{m} \; for \; k = 1, 2, \cdots, m \\
\alpha_S^\sigma &= \Delta t_S / \Delta t_{CS}^\sigma \\
\alpha_S^\tau &= \Delta t_S / \Delta t_{CS}^\tau \\
\beta_{1S}^\sigma = \frac{\alpha_S^\sigma}{6} \left(3\alpha_S^\sigma + \theta (\alpha_S^\sigma)^2 \right), \beta_{2S}^\sigma &= \frac{\theta \alpha_S^\sigma}{6} \left((\alpha_S^\sigma)^2 - 1 \right) \\
\beta_{1S}^\tau = \frac{\alpha_S^\tau}{6} \left(3\alpha_S^\tau + \theta (\alpha_S^\tau)^2 \right), \beta_{2S}^\tau &= \frac{\theta \alpha_S^\tau}{6} \left((\alpha_S^\tau)^2 - 1 \right)
\end{aligned} \tag{22}$$

Since the k-th integration substep in L-domain is not need, we need only (n+1)th integration step as shown in Equation (23).

All element on L-domain at $t^{n+1} = t^n + \Delta t_L = t^n + m\Delta t_S$

$$
\begin{aligned}
\mathbf{u}_L^{n+1} &= \mathbf{u}_L^n + \Delta t_L \dot{\mathbf{u}}_S^n + \beta_{1L}^{\sigma}(\Delta t_{CL}^{\sigma})^2 \ddot{\mathbf{u}}_{L\sigma}^n + \beta_{2L}^{\sigma}(\Delta t_{CL}^{\sigma})^2 \ddot{\mathbf{u}}_{L\sigma}^{n+C_L^{\sigma}} \\
&\quad + \beta_{1L}^{\tau}(\Delta t_{CL}^{\tau})^2 \ddot{\mathbf{u}}_{L\tau}^n + \beta_{2L}^{\tau}(\Delta t_{CL}^{\tau})^2 \ddot{\mathbf{u}}_{L\tau}^{n+C_L^{\tau}} \\
\ddot{\mathbf{u}}_L^{n+1} &= \mathbf{M}_L^{-1}\left(\mathbf{f}_L - \mathbf{K}_L \mathbf{u}_L^{n+1}\right) - \mathbf{M}_L^{-1}\mathbf{B}_L \boldsymbol{\lambda}_L^{n+1} = \tilde{\ddot{\mathbf{u}}}_L^{n+1} - \mathbf{M}_L^{-1}\mathbf{B}_L \boldsymbol{\lambda}_L^{n+1} \\
\ddot{\mathbf{u}}_{L\sigma}^{n+C_L^{\sigma}} &= \tilde{\ddot{\mathbf{u}}}_L^{n+C_L^{\sigma}} - \mathbf{M}_L^{-1}\mathbf{D}_{\sigma}^T \mathbf{B}_S \boldsymbol{\lambda}_L^{n+C_L^{\sigma}} \\
\ddot{\mathbf{u}}_{L\tau}^{n+C_L^{\tau}} &= \tilde{\ddot{\mathbf{u}}}_L^{n+C_L^{\tau}} - \mathbf{M}_L^{-1}\mathbf{D}_{\tau}^T \mathbf{B}_L \boldsymbol{\lambda}_L^{n+C_L^{\tau}} \\
\mathbf{u}_L^{n+C_L^{\sigma}} &= \mathbf{u}_L^n + \Delta t_{CL}^{\sigma} \dot{\mathbf{u}}_L^n + \frac{1}{2}(\Delta t_{CL}^{\sigma})^2 \ddot{\mathbf{u}}_L^n \\
\mathbf{u}_L^{n+C_S^{\tau}} &= \mathbf{u}_L^n + \Delta t_{CL}^{\tau} \dot{\mathbf{u}}_L^n + \frac{1}{2}(\Delta t_{CL}^{\tau})^2 \ddot{\mathbf{u}}_L^n \\
\tilde{\ddot{\mathbf{u}}}_L^{n+1} &= \mathbf{M}_S^{-1}\left(\mathbf{f}_L^{n+1} - \mathbf{K}_L \mathbf{u}_L^{n+1}\right) \\
\tilde{\ddot{\mathbf{u}}}_L^{n+C_L^{\sigma}} &= \mathbf{M}_L^{-1}\left(\mathbf{f}_L^{n+C_L^{\sigma}} - \mathbf{K}_L \mathbf{u}_L^{n+C_L^{\sigma}}\right) \\
\tilde{\ddot{\mathbf{u}}}_L^{n+C_L^{\tau}} &= \mathbf{M}_L^{-1}\left(\mathbf{f}_L^{n+C_L^{\tau}} - \mathbf{K}_L \mathbf{u}_L^{n+C_L^{\tau}}\right) \\
\alpha_L^{\sigma} &= m\Delta t_S / \Delta t_{CL}^{\sigma} = \Delta t_L / \Delta t_{CL}^{\sigma} \\
\alpha_L^{\tau} &= m\Delta t_S / \Delta t_{CL}^{\tau} = \Delta t_L / \Delta t_{CL}^{\tau} \\
\beta_{1L}^{\sigma} = \frac{\alpha_L^{\sigma}}{6}\left(3\alpha_L^{\sigma} + \theta - \theta(\alpha_L^{\sigma})^2\right), \beta_{2L}^{\sigma} &= \frac{\theta\alpha_L^{\sigma}}{6}\left((\alpha_L^{\sigma})^2 - 1\right) \\
\beta_{1L}^{\tau} = \frac{\alpha_L^{\tau}}{6}\left(3\alpha_L^{\tau} + \theta - \theta(\alpha_L^{\tau})^2\right), \beta_{2L}^{\tau} &= \frac{\theta\alpha_L^{\tau}}{6}\left((\alpha_L^{\tau})^2 - 1\right)
\end{aligned}
\tag{23}
$$

As same as one dimensional problem, it is not necessary to consider all of the entire L-domain to satisfy the continuity conditions of Equations (16 and 17) during the k-th integration substep of S-domain. Only 2-layers of L-domain next to the interface boundary have only to satisfy the continuous conditions with S-domain for each substep as shown in Fig. 3. The following equation (24) is k-th substep of 2-layers of L-domain next to the interface boundary.

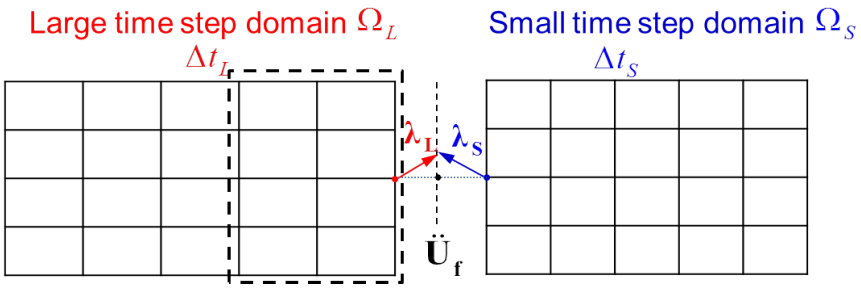

Figure 3. Two layers affecting on the interface loads $\boldsymbol{\lambda}_L$ and $\boldsymbol{\lambda}_S$.

Two layer elements of L-domain adjacent to interface at $t^{n+j} = t^n + k\Delta t_S$

$$
\begin{aligned}
\mathbf{u}_L^{n+j} &= \mathbf{u}_L^n + k\Delta t_S \dot{\mathbf{u}}_L^n + \beta_{1L}^{\sigma}(\Delta t_{CL}^{\sigma})^2 \ddot{\mathbf{u}}_{L\sigma}^n + \beta_{2L}^{\sigma}(\Delta t_{CL}^{\sigma})^2 \ddot{\mathbf{u}}_{L\sigma}^{n+C_L^{\sigma}} \\
&\quad + \beta_{1L}^{\tau}(\Delta t_{CL}^{\tau})^2 \ddot{\mathbf{u}}_{L\tau}^n + \beta_{2L}^{\tau}(\Delta t_{CL}^{\tau})^2 \ddot{\mathbf{u}}_{L\tau}^{n+C_L^{\tau}} \\
\ddot{\mathbf{u}}_L^{n+j} &= \mathbf{M}_L^{-1}\left(\mathbf{f}_L - \mathbf{K}_L \mathbf{u}_L^{n+j}\right) - \mathbf{M}_L^{-1}\mathbf{B}_L \boldsymbol{\lambda}_L^{n+j} = \tilde{\ddot{\mathbf{u}}}_L^{n+j} - \mathbf{M}_L^{-1}\mathbf{B}_L \boldsymbol{\lambda}_L^{n+j} \\
\ddot{\mathbf{u}}_{L\sigma}^{n+C_L^{\sigma}} &= \tilde{\ddot{\mathbf{u}}}_L^{n+C_L^{\sigma}} - \mathbf{M}_L^{-1}\mathbf{D}_{\sigma}^T \mathbf{B}_S \boldsymbol{\lambda}_L^{n+C_L^{\sigma}} \\
\ddot{\mathbf{u}}_{L\tau}^{n+C_L^{\tau}} &= \tilde{\ddot{\mathbf{u}}}_L^{n+C_L^{\tau}} - \mathbf{M}_L^{-1}\mathbf{D}_{\tau}^T \mathbf{B}_L \boldsymbol{\lambda}_L^{n+C_L^{\tau}} \\
\mathbf{u}_L^{n+C_L^{\sigma}} &= \mathbf{u}_L^n + \Delta t_{CL}^{\sigma} \dot{\mathbf{u}}_L^n + \frac{1}{2}(\Delta t_{CL}^{\sigma})^2 \ddot{\mathbf{u}}_L^n \\
\mathbf{u}_L^{n+C_S^{\tau}} &= \mathbf{u}_L^n + \Delta t_{CL}^{\tau} \dot{\mathbf{u}}_L^n + \frac{1}{2}(\Delta t_{CL}^{\tau})^2 \ddot{\mathbf{u}}_L^n \\
\alpha_L^{\sigma} &= k\Delta t_S / \Delta t_{CL}^{\sigma} \\
\alpha_L^{\tau} &= k\Delta t_S / \Delta t_{CL}^{\tau}
\end{aligned}
\tag{24}
$$

Two layers in L-domain are integrated at time ($t^{n+j} = t^n + k\Delta t_S$) on the basis of time ($t^n$), ($t^n + \Delta t_{CL}^{\sigma}$) and ($t^n + \Delta t_{CL}^{\tau}$). Therefore the total calculation time can be reduced by integrating only two layers of L-domain at each substep. The accelerations with 'tilde' in Equation 24 can be obtained as same with Equation 23.
The next step is to find the variables($\boldsymbol{\lambda}_S^{n+j}, \boldsymbol{\lambda}_L^{n+j}, \ddot{\mathbf{u}}_f^{n+j}$) of the interface,$\Gamma_I$. This is equally done by Equations (47 and 48) described in the one-dimensional problem. To do this, We first have to find the interface reaction forces at the critical time in order to obtain those variables. Similar to the one dimensional problem, the order of calculation of the variables on interface, Γ_I, is as follows.

$$
\begin{aligned}
(\boldsymbol{\lambda}_S^{n+jC_S^{\tau}}, \boldsymbol{\lambda}_S^{n+jC_S^{\sigma}}) &\rightarrow \ddot{\mathbf{u}}_S^{n+jC_S} \rightarrow \boldsymbol{\lambda}_S^{n+j} \\
(\boldsymbol{\lambda}_L^{n+C_L^{\tau}}, \boldsymbol{\lambda}_L^{n+C_L^{\sigma}}) &\rightarrow \ddot{\mathbf{u}}_L^{n+C_L} \rightarrow \boldsymbol{\lambda}_L^{n+j}
\end{aligned}
\tag{25}
$$

First, we obtain ($\boldsymbol{\lambda}_S^{n+jC_S^{\tau}}, \boldsymbol{\lambda}_S^{n+jC_S^{\sigma}}$) at the interface of S-domain as follows.

Computation of $\boldsymbol{\lambda}_S^{n+jC_S^{\tau}}$ **at the interface** Γ_I **of S-domain for** $k = 1 : m$

$$
\begin{aligned}
\Delta t \triangleq \Delta t^{\sigma}_{CS} \; .ie. \; \alpha^{\sigma}_{S} = 1 \\
\alpha^{\tau}_{S} = \Delta t^{\sigma}_{CS} / \Delta t^{\tau}_{CS} \\
\beta^{\sigma}_{1S} = 1/2, \; \beta^{\sigma}_{2S} = 0 \\
\mathbf{u}^{n+j}_{S} = \tilde{\mathbf{u}}^{n+j} - \beta^{\tau}_{2S} (\Delta t^{\tau}_{CS})^2 \mathbf{M}^{-1}_{S} \mathbf{D}^{T}_{\tau} \mathbf{B}_{S} \boldsymbol{\lambda}^{n+jC^{\tau}_{S}}_{S} \\
\tilde{\mathbf{u}}^{n+j}_{S} = \mathbf{u}^{n+j_o}_{S} + \Delta t^{\sigma}_{CS} \dot{\mathbf{u}}^{n+j_o}_{S} + \frac{1}{2} (\Delta t^{\sigma}_{CS})^2 \ddot{\mathbf{u}}^{n+j_o}_{S\sigma} + \beta^{\tau}_{1S} (\Delta t^{\tau}_{CS})^2 \ddot{\mathbf{u}}^{n+j_o}_{S\tau} + \beta^{\tau}_{2S} (\Delta t^{\tau}_{CS})^2 \tilde{\ddot{\mathbf{u}}}^{n+jC^{\tau}_{S}}_{S\tau} \\
\mathbf{u}^{n+j^{\sigma}_{CS}}_{f} = \mathbf{u}^{n+j_o}_{f} + \Delta t^{\sigma}_{CS} \dot{\mathbf{u}}^{n+j_o}_{f} + \frac{1}{2} (\Delta t^{\sigma}_{CS})^2 \ddot{\mathbf{u}}^{n+j_o}_{f} \\
\boldsymbol{\lambda}^{n+jC^{\tau}_{S}}_{S} = [\beta^{\tau}_{2S} (\Delta t^{\tau}_{CS})^2 \mathbf{B}^{T}_{S} \mathbf{M}^{-1}_{S} \mathbf{D}^{T}_{\tau} \mathbf{B}_{S}]^{-1} (\mathbf{B}^{T}_{S} \tilde{\mathbf{u}}^{n+j}_{S} - \mathbf{L}_{S} \mathbf{u}^{n+j^{\sigma}_{CS}}_{f})
\end{aligned}
\tag{26}
$$

Computation of $\boldsymbol{\lambda}^{n+jC^{\sigma}_{S}}_{S}$ at the interface Γ_I of S-domain for $k = 1 : m$

$$
\begin{aligned}
\Delta t \triangleq \Delta t^{\tau}_{CS} \; .ie. \; \alpha^{\tau}_{S} = 1 \\
\beta^{\tau}_{1S} = 1/2, \; \beta^{\tau}_{2S} = 0 \\
\mathbf{u}^{n+j}_{S} = \tilde{\mathbf{u}}^{n+j} - \beta^{\sigma}_{2S} (\Delta t^{\sigma}_{CS})^2 \mathbf{M}^{-1}_{S} \mathbf{D}^{T}_{\sigma} \mathbf{B}_{S} \boldsymbol{\lambda}^{n+jC^{\sigma}_{S}}_{S} \\
\tilde{\mathbf{u}}^{n+j}_{S} = \mathbf{u}^{n+j_o}_{S} + \Delta t^{\tau}_{CS} \dot{\mathbf{u}}^{n+j_o}_{S} + \beta^{\sigma}_{1S} (\Delta t^{\sigma}_{CS})^2 \ddot{\mathbf{u}}^{n+j_o}_{S\sigma} + \beta^{\sigma}_{2S} (\Delta t^{\sigma}_{CS})^2 \tilde{\ddot{\mathbf{u}}}^{n+jC^{\sigma}_{S}}_{S\sigma} + \frac{1}{2} \beta^{\tau}_{1S} (\Delta t^{\tau}_{CS})^2 \ddot{\mathbf{u}}^{n+j_o}_{S\tau} \\
\mathbf{u}^{n+j^{\tau}_{CS}}_{f} = \mathbf{u}^{n+j_o}_{f} + \Delta t^{\tau}_{CS} \dot{\mathbf{u}}^{n+j_o}_{f} + \frac{1}{2} (\Delta t^{\tau}_{CS})^2 \ddot{\mathbf{u}}^{n+j_o}_{f} \\
\boldsymbol{\lambda}^{n+jC^{\sigma}_{S}}_{S} = [\beta^{\sigma}_{2S} (\Delta t^{\sigma}_{CS})^2 \mathbf{B}^{T}_{S} \mathbf{M}^{-1}_{S} \mathbf{D}^{T}_{\sigma} \mathbf{B}_{S}]^{-1} (\mathbf{B}^{T}_{S} \tilde{\mathbf{u}}^{n+j}_{S} - \mathbf{L}_{S} \mathbf{u}^{n+j^{\tau}_{CS}}_{f})
\end{aligned}
\tag{27}
$$

we can also get $(\boldsymbol{\lambda}^{n+C^{\tau}_{L}}_{L}, \boldsymbol{\lambda}^{n+C^{\sigma}_{L}}_{L})$ at the interface of L-domain in the similar way as in S-domain. Different thing is to divide into first substep and two or more substep as follows.

Computation of $(\boldsymbol{\lambda}^{n+C^{\tau}_{L}}_{L}, \boldsymbol{\lambda}^{n+C^{\sigma}_{L}}_{L})$ at the interface Γ_I of S-domain for $k = 1 : m$

$$
\begin{aligned}
\Delta t \triangleq \Delta t^{\sigma}_{CL} \\
\Delta t^{'} = \Delta t^{\sigma}_{CL} - (k-1) \Delta t_{S} \\
\mathbf{u}^{n+C^{\tau}_{CL}}_{f} = \mathbf{u}^{n+j_0}_{f} + \Delta t^{'} \dot{\mathbf{u}}^{n+j_0} + \frac{1}{2} (\Delta t^{'})^2 \ddot{\mathbf{u}}^{n+j_0}_{f} \\
\boldsymbol{\lambda}^{n+C^{\tau}_{L}}_{L} = [\beta^{\tau}_{2L} (\Delta t^{\tau}_{CL})^2 \mathbf{B}^{T}_{L} \mathbf{M}^{-1}_{L} \mathbf{D}^{T}_{\tau} \mathbf{B}_{L}]^{-1} (\mathbf{B}^{T}_{L} \tilde{\mathbf{u}}^{n+C^{\tau}_{CL}}_{L} - \mathbf{L}_{CL} \mathbf{u}^{n+C^{\tau}_{CL}}_{f})
\end{aligned}
\tag{28}
$$

$$
\begin{aligned}
\Delta t &\triangleq \Delta t^{\tau}_{CL} \\
\Delta t^{'} &= \Delta t^{\tau}_{CL} - (k-1)\Delta t_S \\
\mathbf{u}_f^{n+C^{\sigma}_{CL}} &= \mathbf{u}_f^{n+j_0} + \Delta t^{'}\dot{\mathbf{u}}^{n+j_0} + \frac{1}{2}(\Delta t^{'})^2\ddot{\mathbf{u}}_f^{n+j_0} \\
\boldsymbol{\lambda}_L^{n+C^{\sigma}_{L}} &= [\beta^{\sigma}_{2L}(\Delta t^{\sigma}_{CL})^2\mathbf{B}_L^T\mathbf{M}_L^{-1}\mathbf{D}_{\sigma}^T\mathbf{B}_L]^{-1}(\mathbf{B}_L^T\tilde{\mathbf{u}}_L^{n+C^{\sigma}_{CL}} - \mathbf{L}_L\mathbf{u}_f^{n+C^{\sigma}_{CL}})
\end{aligned}
\tag{29}
$$

$$
\begin{bmatrix} \mathbf{B}_L^T\mathbf{M}_L^{-1}\mathbf{B}_L & 0 & \mathbf{L}_L \\ 0 & \mathbf{B}_S^T\mathbf{M}_S^{-1}\mathbf{B}_S & \mathbf{L}_S \\ \mathbf{L}_L^T & \mathbf{L}_S^T & 0 \end{bmatrix} \begin{bmatrix} \boldsymbol{\lambda}_L \\ \boldsymbol{\lambda}_S \\ \mathbf{u}_f \end{bmatrix}^{n+j} = \begin{bmatrix} \mathbf{B}_L^T\tilde{\ddot{\mathbf{u}}}_L^{n+j} \\ \mathbf{B}_S^T\tilde{\ddot{\mathbf{u}}}_S^{n+j} \\ 0 \end{bmatrix} \; for\; k = 1 : m\; on\; \Gamma_I \tag{30}
$$

$(\boldsymbol{\lambda}_S^{n+jC^{\sigma}_S}, \boldsymbol{\lambda}_S^{n+jC^{\tau}_S})$ are calculated explicitly in every substep as shown in Equations (26- 27). And $(\boldsymbol{\lambda}_L^{n+C^{\sigma}_L}, \boldsymbol{\lambda}_L^{n+C^{\tau}_L})$ of interface Γ_I should be also updated in every substep as shown in Equations (28-29) because $(\boldsymbol{\lambda}_S^{n+jC^{\sigma}_S}, \boldsymbol{\lambda}_S^{n+jC^{\tau}_S})$ are recalculated in each substep. And then, $(\boldsymbol{\lambda}_L^{n+j}, \boldsymbol{\lambda}_S^{n+j}, \mathbf{u}_f^{n+j})$ are calculated at each interface nodes as shown in Equation (30).
There is also a alternative method for obtaining $(\boldsymbol{\lambda}_S^{n+jC^{\sigma}_S}, \boldsymbol{\lambda}_S^{n+jC^{\tau}_S})$ and $(\boldsymbol{\lambda}_L^{n+C^{\sigma}_L}, \boldsymbol{\lambda}_L^{n+C^{\tau}_L})$, which is to use a extrapolation by linear convex combination as following Equations (31- 32) as a similar way with reference [18].

Alternative method of computing $(\boldsymbol{\lambda}_S^{n+jC^{\sigma}_S}, \boldsymbol{\lambda}_S^{n+jC^{\tau}_S})$ on S-domain

$$
\begin{aligned}
\alpha_{\sigma} &= \Delta t_S/\Delta t^{\sigma}_{CS} \\
\alpha_{\tau} &= \Delta t_S/\Delta t^{\tau}_{CS} \\
\boldsymbol{\lambda}_S^{n+j} &= (1-\alpha_{\sigma})\boldsymbol{\lambda}_S^{n+(j-1)} + \alpha_{\sigma}\boldsymbol{\lambda}_S^{n+jC^{\sigma}_S} \\
\boldsymbol{\lambda}_S^{n+j} &= (1-\alpha_{\tau})\boldsymbol{\lambda}_S^{n+(j-1)} + \alpha_{\tau}\boldsymbol{\lambda}_S^{n+jC^{\tau}_S}
\end{aligned}
\tag{31}
$$

Alternative method of computing $(\boldsymbol{\lambda}_L^{n+C^{\sigma}_L}, \boldsymbol{\lambda}_L^{n+C^{\tau}_L})$ on L-domain

$$
\begin{aligned}
\alpha_{\sigma} &= k\Delta t_S/\Delta t^{\sigma}_{CL} \\
\alpha_{\tau} &= k\Delta t_S/\Delta t^{\tau}_{CL} \\
\boldsymbol{\lambda}_L^{n+j} &= (1-\alpha_{\sigma})\boldsymbol{\lambda}_L^{n} + \alpha_{\sigma}\boldsymbol{\lambda}_L^{n+C^{\sigma}_L} \\
\boldsymbol{\lambda}_L^{n+j} &= (1-\alpha_{\tau})\boldsymbol{\lambda}_L^{n} + \alpha_{\tau}\boldsymbol{\lambda}_L^{n+C^{\tau}_L}
\end{aligned}
\tag{32}
$$

However, our numerical experiment using the alternative method showed that $\boldsymbol{\lambda}_S^{n+j} \neq \boldsymbol{\lambda}_L^{n+j}$ in case of $\Delta t_{CL}^{\sigma} >> \Delta t_{CS}^{\sigma}$. So, we did not adopted the alternative method for obtaining more accurate solution in the present algorithm. Despite our present is shown as more or less complicated, the present algorithm has the advantage that the calculation time is drastically reduced since L-domain is computed only in two elements next to the internal interface at each substep, and that the solution is more accurate specially in case of $\Delta t_{CL}^{\sigma} >> \Delta t_{CS}^{\sigma}$ Finally, we describe the flowchart of the multistep time integration for multidimensional problem.

Flowchart of multistep time integration for two-dimensional heterogeneous solids

Start of Main Step $n = 1 : N$ on L-domain

Step 1 : Prepare $(\mathbf{u}_L^n, \dot{\mathbf{u}}_L^n, \ddot{\mathbf{u}}_L^n)$

Start of Substep $k = 1 : m$ on S-Domain

Step 2 : Prepare $(\mathbf{u}_S^{n+j_o}, \dot{\mathbf{u}}_S^{n+j_o}, \ddot{\mathbf{u}}_S^{n+j_o})$
Step 2.1 : Compute $(\boldsymbol{\lambda}_S^{n+jC_S^{\sigma}}, \boldsymbol{\lambda}_S^{n+jC_S^{\tau}}, \boldsymbol{\lambda}_L^{n+C_L^{\sigma}}, \boldsymbol{\lambda}_L^{n+C_L^{\tau}}\ and\ \ddot{\mathbf{u}}_f^{n+j})$ at the interface, Γ_I
Step 2.1.1 : Compute $(\boldsymbol{\lambda}_S^{n+jC_S^{\sigma}}, \boldsymbol{\lambda}_S^{n+jC_S^{\tau}})$
Step 2.1.2 : Compute $\boldsymbol{\lambda}_L^{n+C_L^{\sigma}}, \boldsymbol{\lambda}_L^{n+C_L^{\tau}})$
Step 2.2 : Compute $(\boldsymbol{\lambda}_S^{n+j}, \boldsymbol{\lambda}_L^{n+j}\ and\ \ddot{\mathbf{u}}_f^{n+j})$
Step 2.3 : Compute $(\dot{\mathbf{u}}_S^{n+j}, \ddot{\mathbf{u}}_S^{n+j)})$

$$\begin{aligned} \ddot{\mathbf{u}}_S^{n+j} &= \tilde{\ddot{\mathbf{u}}}_S^{n+j} - \mathbf{M}_S^{-1}\mathbf{B}_S\boldsymbol{\lambda}_S^{n+j} \\ \dot{\mathbf{u}}_S^{n+j} &= \dot{\mathbf{u}}_S^{n+(j-1)} + \Delta t_S\{(1-\gamma)\ddot{\mathbf{u}}_S^{n+(j-1)} + \gamma\ddot{\mathbf{u}}_S^{n+j}\} \end{aligned} \tag{33}$$

Step 2.4 : Update $(\mathbf{u}_f^{n+j}, \dot{\mathbf{u}}_f^{n+j)})$ and $(\dot{\mathbf{u}}_S^{n+j}, \ddot{\mathbf{u}}_S^{n+j)})$ at the interface, Γ_I

$$\begin{aligned} \dot{\mathbf{u}}_f^{n+j} &= \dot{\mathbf{u}}_f^{n+(j-1)} + \Delta t_S\{(1-\gamma)\ddot{\mathbf{u}}_f^{n+(j-1)} + \gamma\ddot{\mathbf{u}}_f^{n+j}\} \\ \mathbf{u}_f^{n+j} &= \mathbf{u}_f^{n+(j-1)} + \Delta t_S\dot{\mathbf{u}}_f^{n+j} \end{aligned} \tag{34}$$

END of Substep on S-Domain

Step 3 : Compute $(\dot{\mathbf{u}}_L^{n+1}, \ddot{\mathbf{u}}_L^{n+1)})$ on entire L-domain
Step 3.1 : Compute $(\dot{\mathbf{u}}_L^{n+1}, \ddot{\mathbf{u}}_L^{n+1)})$

$$\begin{aligned} \ddot{\mathbf{u}}_L^{n+1} &= \tilde{\ddot{\mathbf{u}}}_L^{n+1} - \mathbf{M}_L^{-1}\mathbf{B}_L\boldsymbol{\lambda}_L^{n+1} \\ \dot{\mathbf{u}}_L^{n+1} &= \dot{\mathbf{u}}_L^{n} + \Delta t_L\{(1-\gamma)\ddot{\mathbf{u}}_L^{n} + \gamma\ddot{\mathbf{u}}_L^{n+1}\} \end{aligned} \tag{35}$$

Step 3.2 : Update $(\mathbf{u}_L^{n+1}, \dot{\mathbf{u}}_L^{n+1)})$ only at the interface, Γ_I, to prevent the drifting of the interface

$$\begin{aligned} \mathbf{L}_L \mathbf{u}_L^{n+1} &= \mathbf{B}_L^T \mathbf{u}_f^{n+1} \\ \mathbf{L}_L \dot{\mathbf{u}}_L^{n+1} &= \mathbf{B}_L^T \dot{\mathbf{u}}_f^{n+1} \end{aligned} \tag{36}$$

END of Main Step on L-domain

4. NUMERICAL EXPERIMENTS

We choose 3-problems of discontinuous elastic wave propagation in heterogeneous solids to demonstrate the salient features of the present algorithm: two kinds problems of one dimensional heterogeneous rods and a crack tip problems subjected to mode-II loadings in a heterogeneous solid with plane strain condition. The simulation of the crack tip problems is chosen because various types of waves, including Rayleigh and Schmidt waves, will emanate from the crack tip and these waves have high singularities at the crack tip.

4.1. Stress wave propagated from L-domain to S-domain in one-dimensional heterogeneous rod

As a first example, we have chosen the stress wave propagation problem in a rod consisting of two materials (See Appendix for the details of the present algorithm for one-dimensional case). As shown in Fig. 4, the one-dimensional rod consists of a soft material on the left(length=50mm, density=8000 kg/m^3, the number of element=300) and a hard material on the right(length=50mm, density=8000 kg/m^3, the number of element=300). Since the elastic modulus of each material is 0.02GPa and 200GPa, the propagation speed of the stress wave is 50 m/s and 5000 m/s, respectively. Thus, if the element sizes are equal in all elements of the two materials, the ratio of their critical time steps is 100. The boundary condition is fixed at the right end as shown in Fig. 4. The initial velocity of 10 m/s was imposed at the left end to allow the stress wave to propagate from the soft material(L-domain) to the hard material(S-domain).
Fig. 5 shows the approximate solutions at time=$2600\mu s$ and $3800\mu s$ rescpectively, in terms of the velocity distribution along the two materials. If the incident stress wave propagated from left side end reaches to the interface(x=50mm), it is partially transmitted to the right side end and partially reflected to left side end. Since the impedance difference between two materials is high, the amplitude of the transmitted wave is small. Therefore, the small transmitted wave is propagated to the right side end, and then reflected to the left soft material. As a result, the stress wave in a left soft material always contains the small oscillations as shown in Fig. 5.

First, Fig. 6 shows the results of the conventional central difference method(CDM) as applied with a single step integration and without partitioning, which exhibit the deleterious pre-shock dispersion errors. It should be noted that at time $t = 2600\mu s$ (shown at the left) the incoming wave is propagating from the left to the right, and at time $t = 3600\mu s$ the wave is reflecting back from the right fixed end. The same problem analyzed by the the push-forward-pullback time integration method [13] without employing the partitioned equations motion is shown in Fig. 7, which shows a significant reduction in spurious oscillations for both the incoming and reflecting waves.

Second, the same problem is now partitioned via the method of Lagrange multipliers, and analyzed by single time integration employing the central difference method and the push-forward-pullback time

integration method(detailed in Appendix), respectively. Figure 8 shows a similar level of dispersion errors in the case of the central difference method. On the other hand, Fig. 9 shows the our present method maintains a similar level of improved spurious oscillations comparable to that of non-partitioned case shown in Fig. 7.

Third, the same problem is analyzed by partitioned, multistep integration algorithm. It should be noted that the domain for the large time step is integrated only once whereas that for the small time step domain is integrated 100 times. This saving of computational effort about 50%, shown in Fig. 10 for the central difference method and Fig. 11 for the push-forward and pullback integration method.

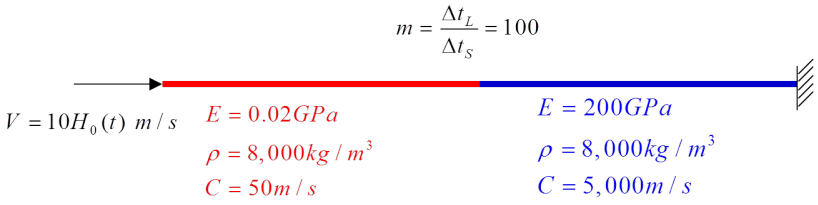

Figure 4. One-dimensional problem for the stress wave propagated from L-domain to S-domain

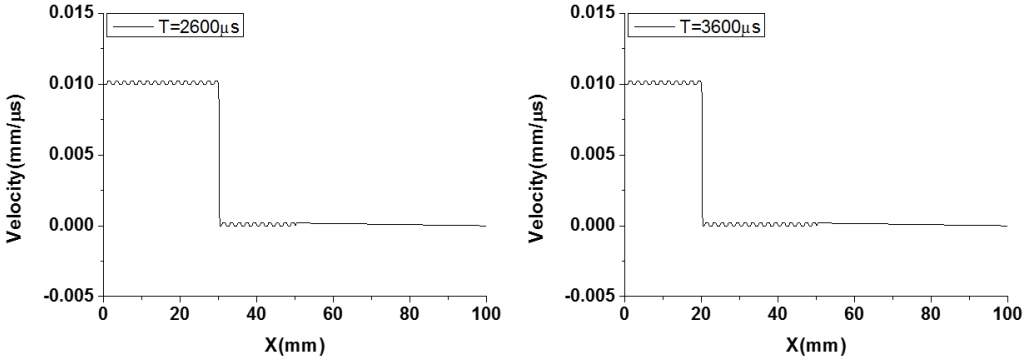

Figure 5. One-dimensional problem for the stress wave problem propagated from L-domain to S-domain at $t = 2600\mu s$ and $3800\mu s$: Approximate Solutions obtained from x-t diagram.

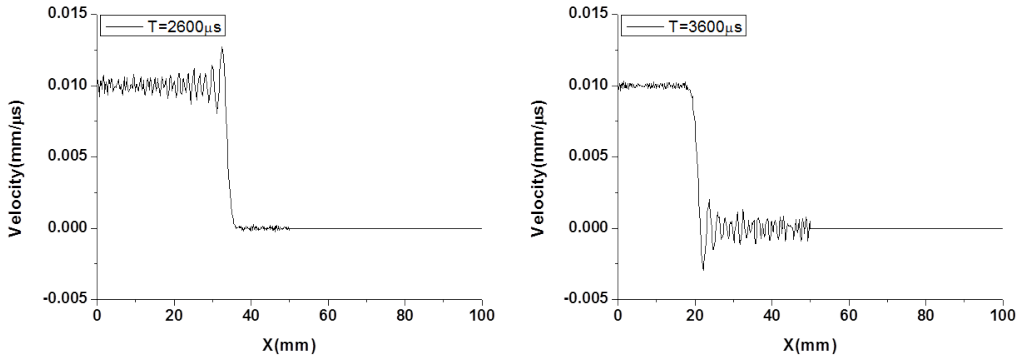

Figure 6. One-dimensional problem for the stress wave problem propagated from L-domain to S-domain at $t = 2600\mu s$ and $3800\mu s$: Central Difference Method(Single step) without partitioning.

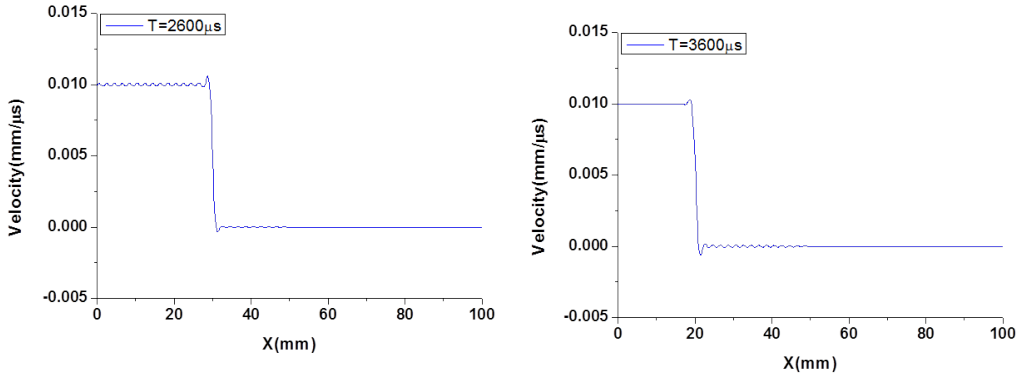

Figure 7. One-dimensional problem for the stress wave problem propagated from L-domain to S-domain at $t = 2600\mu s$ and $3800\mu s$: Push-forward Pullback Time Integration(Single step) without partitioning.

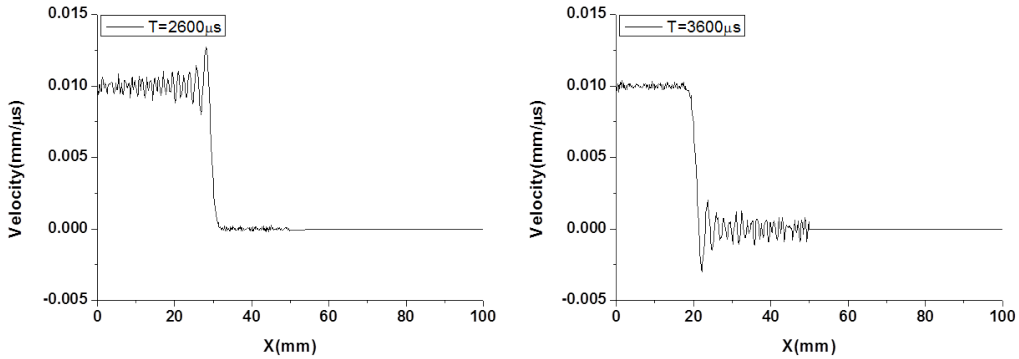

Figure 8. One-dimensional problem for the stress wave problem propagated from L-domain to S-domain at $t = 2600\mu s$ and $3800\mu s$: Central Difference Method(Single step) with Partitioned Interface.

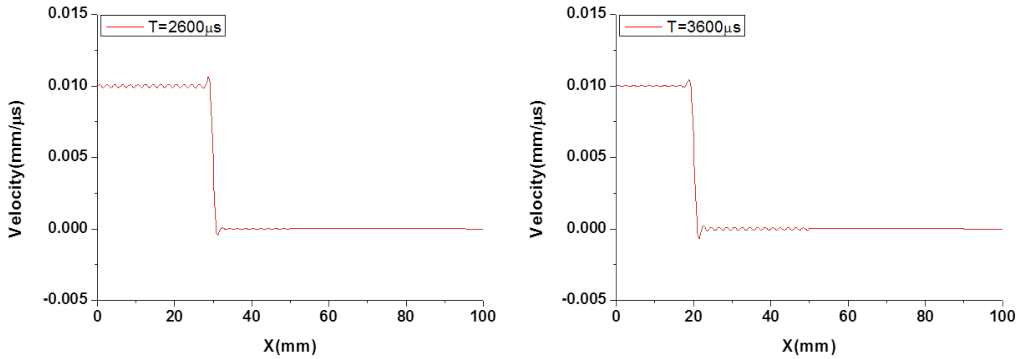

Figure 9. One-dimensional problem for the stress wave problem propagated from L-domain to S-domain at $t = 2600\mu s$ and $3800\mu s$: Push-forward Pullback Time Integration(Single step) with Partitioned Interface.

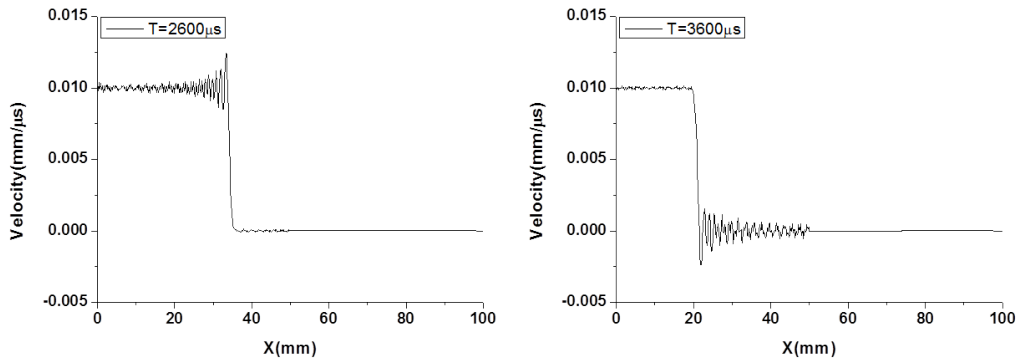

Figure 10. One-dimensional problem for the stress wave problem propagated from L-domain to S-domain at $t = 2600\mu s$ and $3800\mu s$: Central Difference Method(Multistep) with Partitioned Interface.

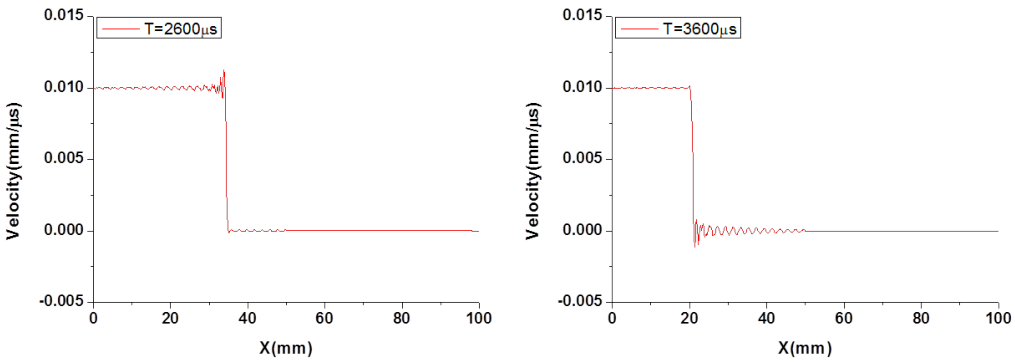

Figure 11. One-dimensional problem for the stress wave problem propagated from L-domain to S-domain at $t = 2600\mu s$ and $3800\mu s$: Push-forward Pullback Time Integration(Multistep) with Partitioned Interface.

4.2. Stress wave propagated from S-domain to L-domain in one-dimensional heterogeneous rods

As in the first example, the second example is a stress wave propagation problem in a rod made of two heterogeneous materials. Since the properties of the two materials are the same as in the first example, the ratio of their critical time steps is also 100. In contrast to the first example, the boundary condition is fixed at the left end as shown in Fig. 12 and the initial velocity of 10 m/s is imposed at the right end. Thus, the stress wave propagates from the harder material(S-domain) toward the weaker material(L-domain).

Fig. 13 shows the approximate solutions at time=$33\mu s$ and $180\mu s$ rescpectively, which are the velocity distribution along the two materials. If the incident stress wave propagated from right side end reaches to the interface(x=50mm), it is partially transmitted to the left side end and partially reflected to left side end. Due to the impedance difference between two materials, the velocity amplitude of the transmitted wave is about 2-times than the incident wave and its wave length is 1mm. As a result, the rectangualr shaped stress wave with 1mm of wave length is generated and propagated to the left soft material as shown in Fig. 13.

First, Fig. 14 shows the results of the conventional central difference method(CDM) as applied with a single step integration and without partitioning, which exhibit the deleterious pre-shock dispersion errors. It should be noted that at time $t = 33\mu s$ (shown at the left) the first reflecting wave is propagating from the right to the left, leaving a sharp discontinuity at the interface ($50mm$). At time $t = 180\mu s$ the wave have been reflecting several times back and forth from the left fixed end. The same problem analyzed by the the push-forward-pullback time integration method [13] without employing the partitioned equations motion is shown in Fig. 15, which shows a significant reduction in spurious oscillations for both the incoming and reflecting waves..

Second, the same problem is now partitioned via the method of Lagrange multipliers, and analyzed by single time integration employing the central difference method and the push-forward-pullback time integration method(detailed in Appendix), respectively. Figure 16 shows a similar level of dispersion errors in the case of the central difference method. On the other hand, Fig. 17 shows the our present method maintains a similar level of improved spurious oscillations comparable to that of non-partitioned case shown in Fig. 15.

Third, the same problem is analyzed by partitioned, multistep integration algorithm. It should be noted, once again, that the domain for the large time step is integrated only once whereas that for the small time step domain is integrated 100 times. This saving of computational effort about 50%, shown in Fig. 18 for the central difference method and Fig. 19 for the push-forward and pullback integration method.

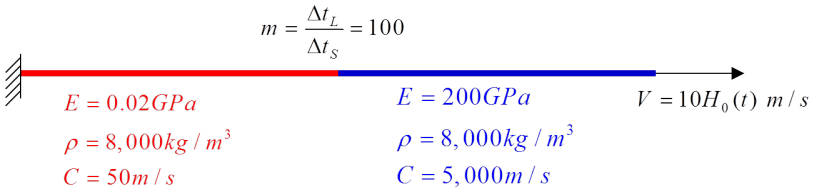

Figure 12. One-dimensional problem for the stress wave propagated from S-domain to L-domain

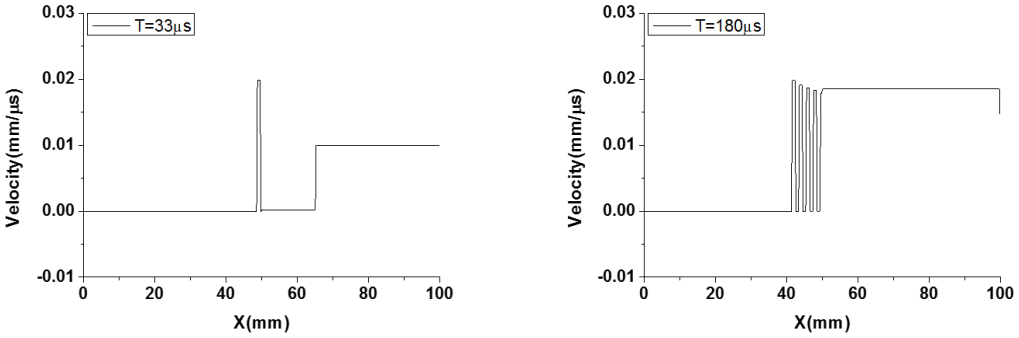

Figure 13. One-dimensional problem for the stress wave problem propagated from S-domain to L-domain at $t = 33\mu s$ and $180\mu s$: Approximate Solutions obtained from x-t diagram.

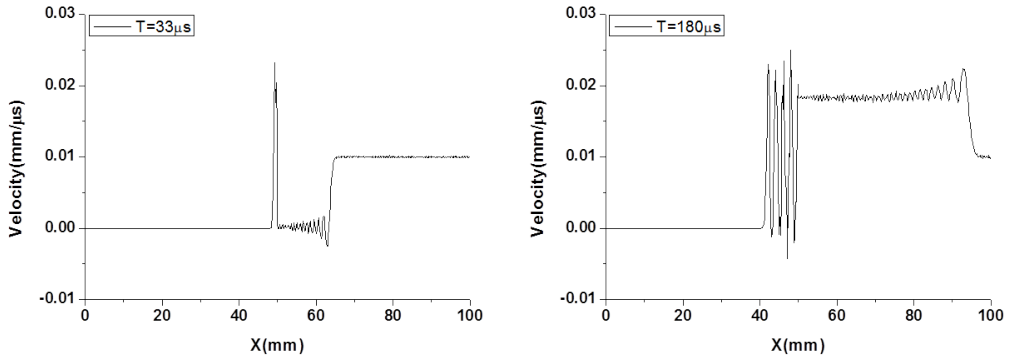

Figure 14. One-dimensional problem for the stress wave problem propagated from S-domain to L-domain at $t = 33\mu s$ and $180\mu s$: Central Difference Method(Single step) without partitioning.

The preceding two one-dimensional wave propagation through heterogeneous materials analyzed by the present multistep integration algorithm indicates that the proposed partitioned multistep explicit integration algorithm is accurate and efficient compared to the conventional central difference method-based multistep results.

We now proceed to an analysis of discontinuous wave propagation through two-dimensional heterogeneous materials.

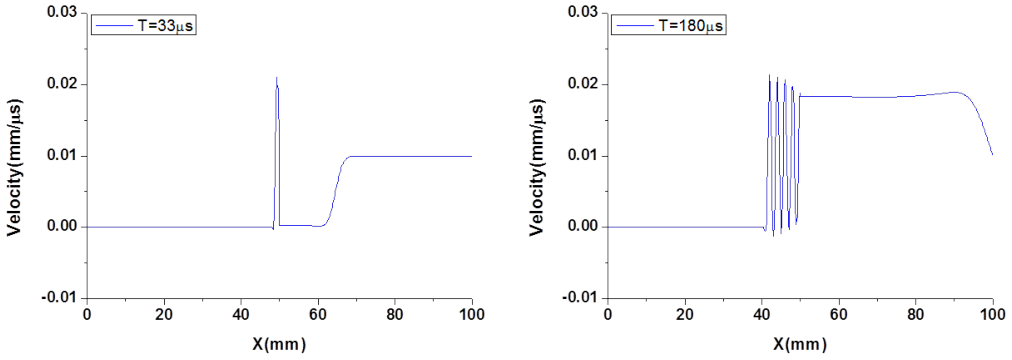

Figure 15. One-dimensional problem for the stress wave problem propagated from S-domain to L-domain at $t = 33\mu s$ and $180\mu s$: Pushforward Pullback Time Integration(Single step) without partitioning.

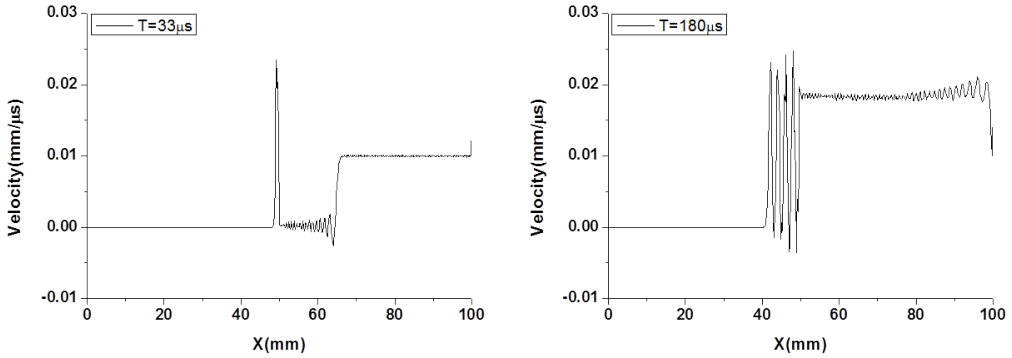

Figure 16. One-dimensional problem for the stress wave problem propagated from S-domain to L-domain at $t = 33\mu s$ and $180\mu s$: Central Difference Method(Single step) with Partitioned Interface.

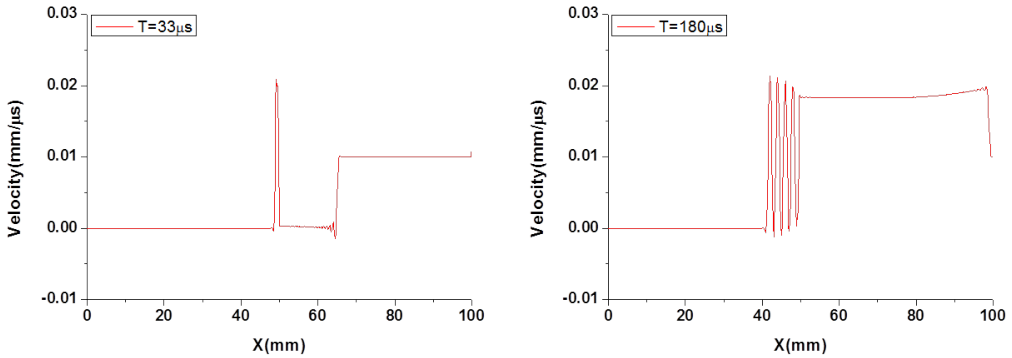

Figure 17. One-dimensional problem for the stress wave problem propagated from S-domain to L-domain at $t = 33\mu s$ and $180\mu s$: Push-forward Pullback Time Integration(Single step) with Partitioned Interface.

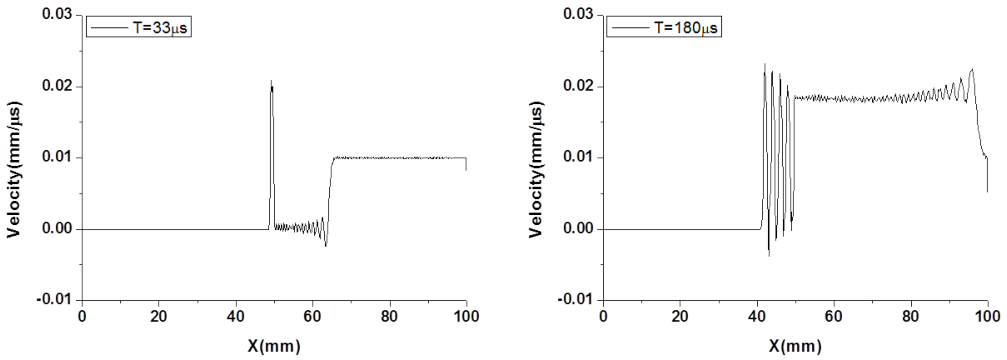

Figure 18. One-dimensional problem for the stress wave problem propagated from S-domain to L-domain at $t = 33\mu s$ and $180\mu s$: Central Difference Method(Multistep) with Partitioned Interface.

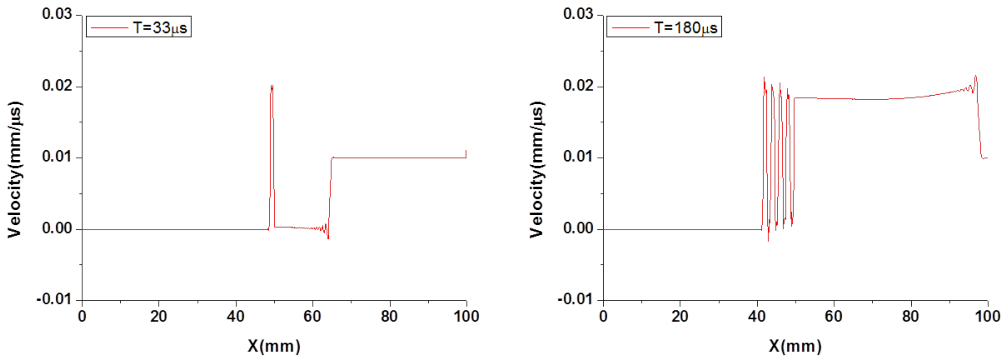

Figure 19. One-dimensional problem for the stress wave problem propagated from S-domain to L-domain at $t = 33\mu s$ and $180\mu s$: Push-forward Pullback Time Integration(Multistep) with Partitioned Interface.

4.3. Crack tip at the center of heterogeneous plate subjected to mode-II type incident wave

A plane strain problem with crack tip between the heterogeneous solids is subjected to a mode-II type incident wave as shown in Fig. 20. The upper part of the plate is a hard material and the lower part is a soft material. Since the elastic modulus of each material is 200GPa and 2GPa, the ratio of the critical time step sizes is equal to 10 if the two materials have the same element size. Figure 21 show the results of maximum shear stress contour plots of the conventional central difference method with a single step integration for both the stiff and soft (upper half and lower half in Fig. 20) portion of the structure. Notice that the central difference method fails to exhibits the surface wave (viz., Rayleigh wave and von-Schmidt waves) in the stiff portion of the structure as shown in Fig. 21(a). Even for the lower soft part of the structure, significant computational dispersion is detected as illustrated in Fig. 21(b). This is clearly manifested when compared with the results obtained by the push-forward pullback time integration as shown in Fig. 22(a,b), which clearly demonstrate the surface waves propagating in the upper stiff portion and relatively minor dispersion in the lower soft portion.

Results for a single step integration with the partitioned equations of motion are shown in Figs. 23 and 24. Their results are similar to those reported in Figs. 21 and 22 with the same single time integration without partitioning.

Multistep integration with the partitioned equations of motion via the method of Lagrange multipliers has been carried out, employing both the central difference method and the push-forward and pullback integration method. Figures 25 and 26 illustrate that the results are similar to those of the partitioned single step integration as shown in Figs. 23 and 24. There is some degrees of dissipation of the energy being carried away by the surface waves, but not significant enough to affect the principal portion of the energy associated with shear stress waves.

Finally, maximum shear stress distributions across the cross section at $X = 0.75mm$ are plotted in Figs. 27 and 28 for two different times, $t = 0.97\mu s$ and $t = 2.26\mu s$. In an earlier work [14], it was demonstrated that the push-forward and pull-back integration method outperforms several explicit methods in terms of capturing the predominant shear stress wave magnitudes. The same superior performance is demonstrated in the case of shear stress wave propagation through heterogeneous materials as shown in Figs. 27 and 28 , where we take the result of the push-forward and pull-back integration method with single integration step as a reference solution. The example case is for the critical time ratio of 10. Although note reported herein, we have carried out for a case of the critical time step ratio up to 100, a similar improvement by the proposed algorithm has been observed without numerical difficulties such as divergence or outright instability. For completeness, we report that a high mode oscillation appearing in the stiff zone (the blue line between $0 < x < 0.4$ in Fig. 28) is observed, which we conjecture a presence of surface waves emanating from the singular crack tip. While it carries only a small percentage of the total system wave energy, a more detailed investigation is under way. If it turns out to be important phenomena, we will report in a future communication.

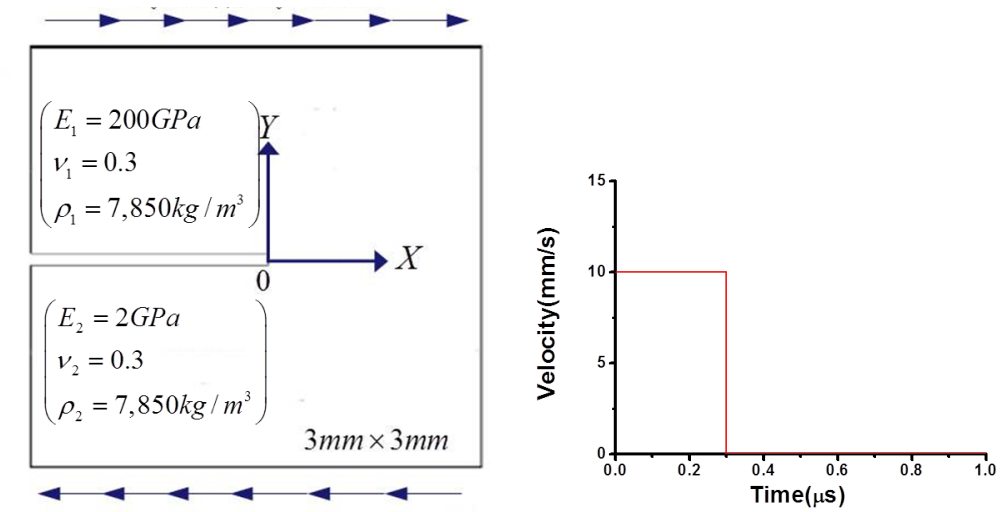

(a) (b)

Figure 20. Plane strain rectangular model(mode-II) with initial crack tip subjected to a Heaviside initial velocity input: (a) geometry and boundary conditions; (b) imposed velocity.

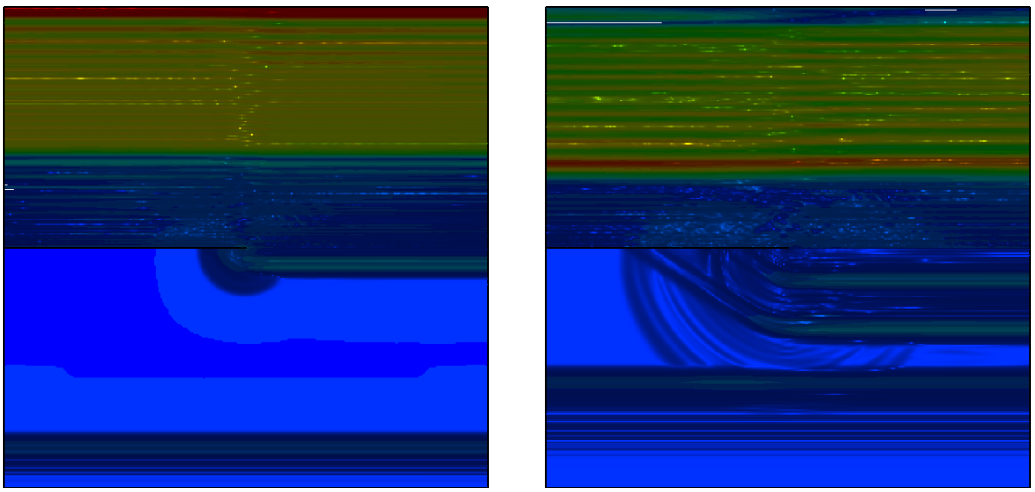

(a) (b)

Figure 21. Maximum shear stress contour plots of Central Difference Method(Single step) without partitioning: (a) $t = 0.97\mu s$;(b) $t = 2.26\mu s$.

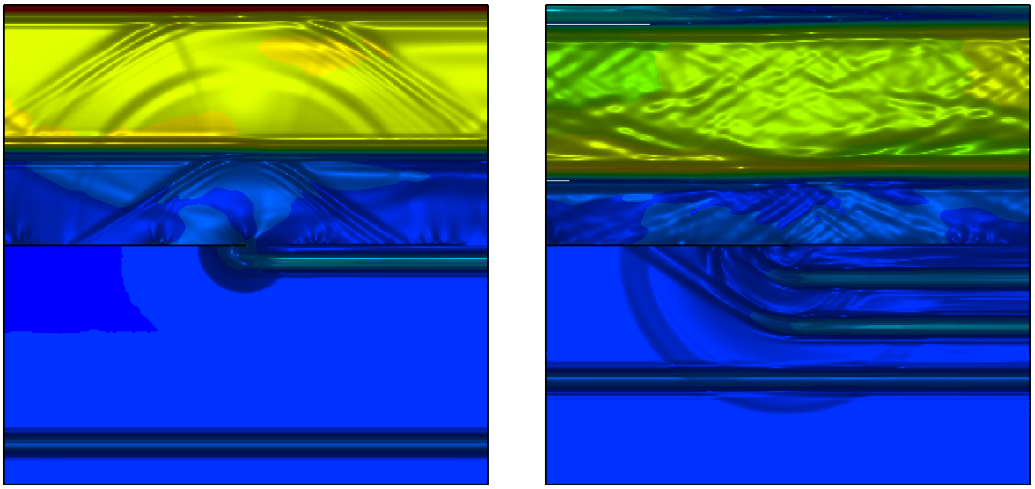

(a) (b)

Figure 22. Maximum shear stress contour plots of Push-forward Pullback Time Integration(Single step) without partitioning: (a) $t = 0.97\mu s$;(b) $t = 2.26\mu s$.

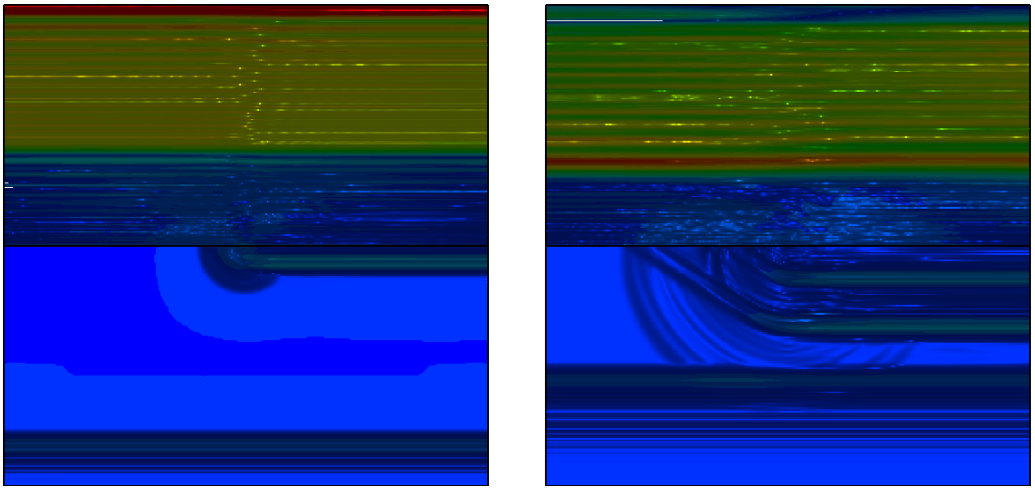

(a) (b)

Figure 23. Maximum shear stress contour plots of Central Difference Method(Single step) with Partitioned Interface: (a) $t = 0.97\mu s$;(b) $t = 2.26\mu s$.

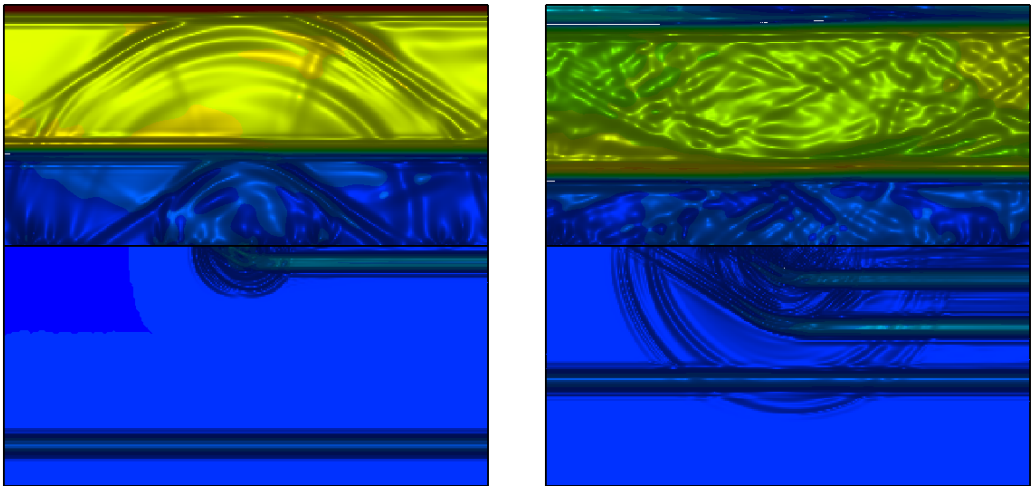

(a) (b)

Figure 24. Maximum shear stress contour plots of Push-forward Pullback Time Integration(Single step) with Partitioned Interface: (a) $t = 0.97\mu s$;(b) $t = 2.26\mu s$.

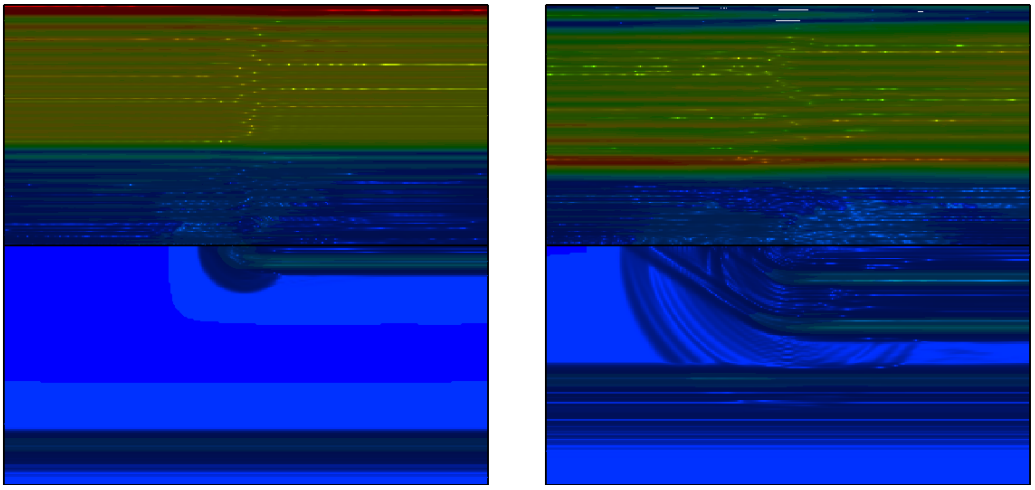

(a) (b)

Figure 25. Maximum shear stress contour plots of Central Difference Method(Multistep) with Partitioned Interface: (a) $t = 0.97\mu s$;(b) $t = 2.26\mu s$.

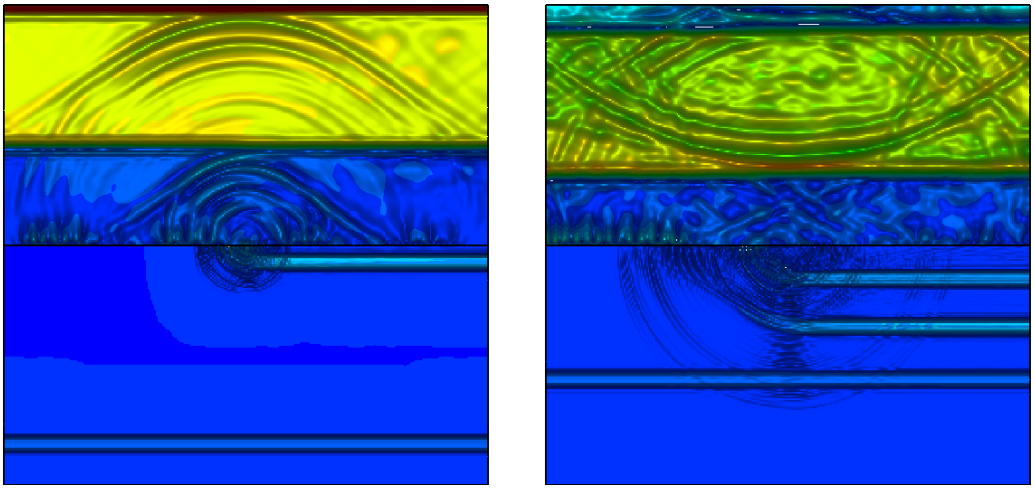

(a) (b)

Figure 26. Maximum shear stress contour plots of Push-forward Pullback Time Integration(Multistep) with Partitioned Interface: (a) $t = 0.97\mu s$;(b) $t = 2.26\mu s$.

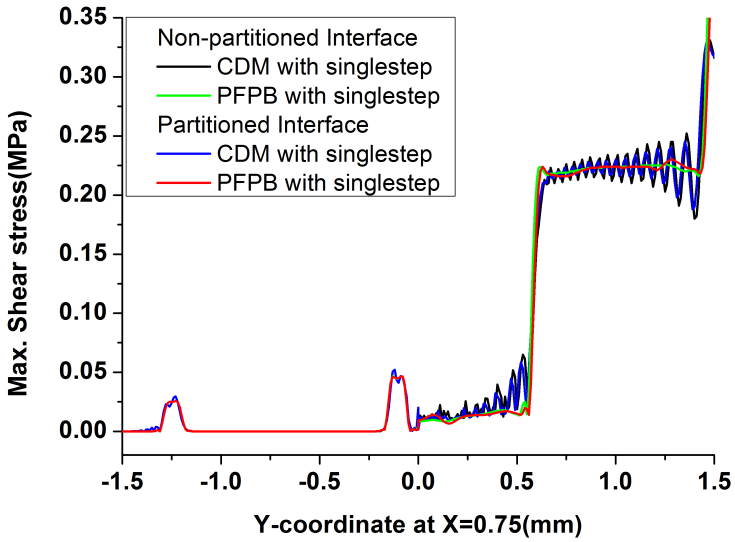

(a)

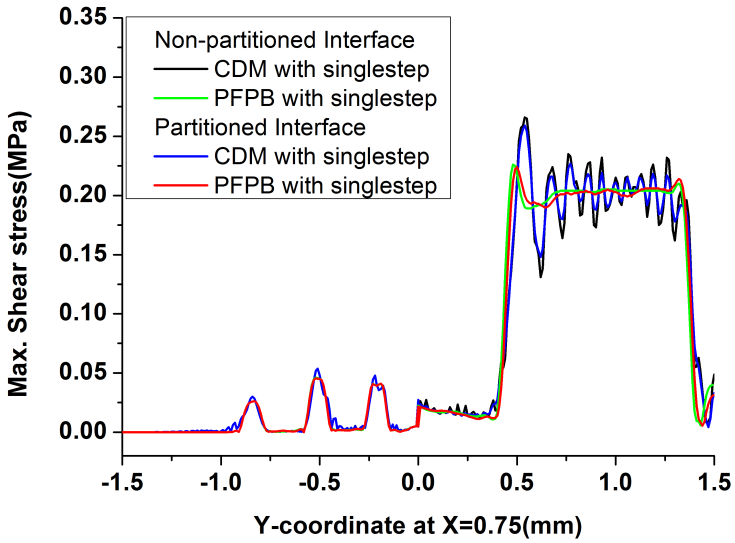

(b)

Figure 27. Comparison results of the maximum shear stress distribution along Y-axis at X=0.75(mode-II problem) between Partitioned interface and Non-partitioned Interface: (a) $t = 0.97\mu s$;(b) $t = 2.26\mu s$. PFPB stands for Push-Forward and Pull-Back integration method.

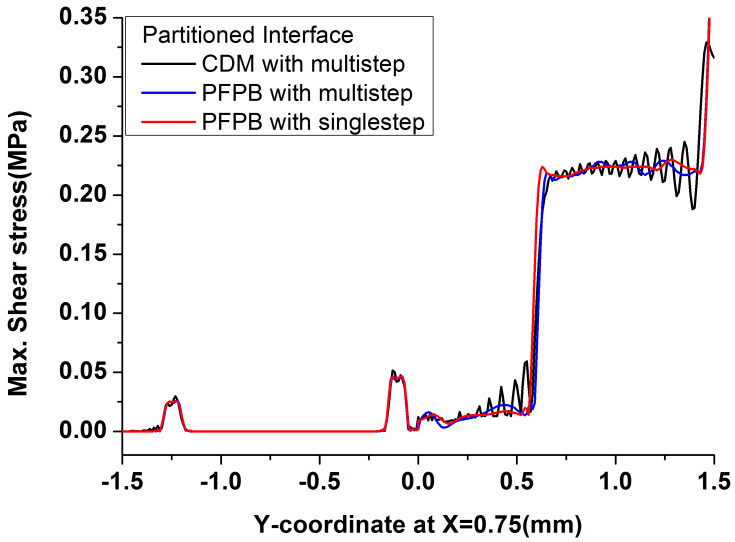

(a)

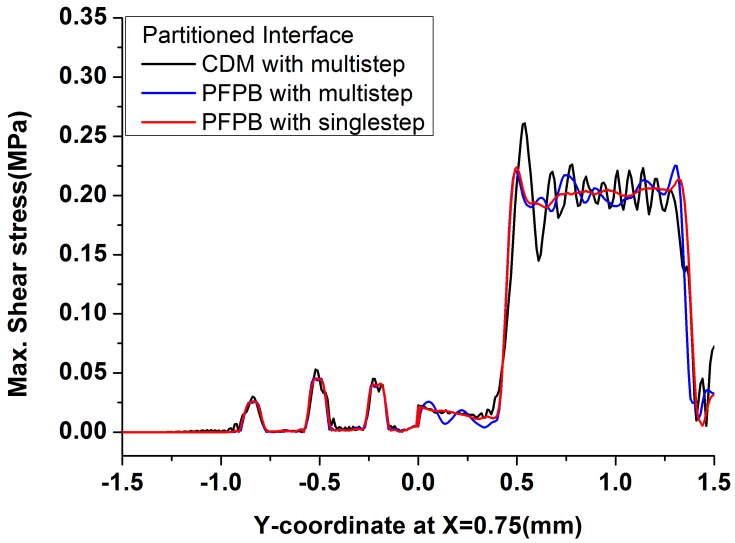

(b)

Figure 28. Comparison results of the maximum shear stress distribution along Y-axis at X=0.75(mode-II problem) between Single step and Multistep Time Integration with Partitioned Interface: (a) $t = 0.97\mu s$;(b) $t = 2.26\mu s$. PFPB stands for Push-Forward and Pull-Back integration method.

5. CONCLUSIONS

An explicit-explicit multistep time integration algorithm for computing the discontinuous stress wave propagation for heterogeneous solids is presented. The proposed algorithm reduces the front-shock and post-shock vibrations of discontinuous stress waves and accurately calculates the wave front propagated at various speeds in heterogeneous solids. The present algorithm stays robust up to 100 critical times step ratio and the results are comparable with those integrated with a single critical step of the stiff materials, thus leading to significant computational savings. While considered for only two domain problems, when the proposed algorithm would offer significant computational savings for heterogeneities with several domains. This present study has been restricted to the derivation of the algorithm and the demonstraion for one and two dimensional problems, however, we hope to report the stability and accuracy analyses in the near future.

Acknowledgements

This work was partially supported by the Nuclear Safety Research Program through the Korea Foundation of Nuclear Safety(KOFONS), granted financial resource from the Nuclear Safety and Security Commission(NSSS), Republic of Korea(No.1403013). The work of R. Kolman was supported by the Centre of Excellence for nonlinear dynamic behavior of advanced materials in engineering CZ.02.1.01/0.0/0.0/15 003(0000493) (Excellent Research Teams) in the framework of Operational Program Research, Development and Education, and the grant project of the Czech Science Foundation, 17-22615S, within institutional support RVO:61388998.

REFERENCES

1. H. Kolsky. Stress waves in solids. *Dover Publications* New York 1963.
2. I. Harari. Special issue on new computational methods for wave propagation. *Wave Motion* 2004; **39**(4):279–280.
3. W. H. Reed, T. R. Hill. Triangular mesh methods for the neutron transport equation. *Tech. Report LA-UR-73-479, Los Alamos Scientific Labaratory* 1973.
4. Hughes TJR, Hulbert GM. Space-time finite element methods for elastodynamics: Formulations and error estimates. *Computer Methods in Applied Mechanics and Engineering* 1988; **66** :339–363.
5. Hulbert GM, Hughes TJR. Space-time finte element methods for second order hyperbolic equations. *Computer Methods in Applied Mechanics and Engineering* 1990; **84** :327–347.
6. Huang H, Costanzo F. On the use of space-time finite elements in the solution of elasto-dynamic problems with strain discontinuities. *Computer Methods in Applied Mechanics and Engineering* 2002; **191** :5315–5343.
7. J. M. Wendlandt, J. E. Marsden. Mechanical integrators derived from a discrete variational principle. *Physica D* 1997; **106** :223–246.
8. Kane C., Marsden JE, Ortiz M, and M. West M. Variational integrators and the Newmark algorithm for conservative and dissipative mechanical systems. *International Journal for Numerical Methods in Engineering* 2000; **49**:1295–1325.
9. Cho SS, Huh H, Park KC. A time-discontinuous implicit variational integrator for stress wave propagation analysis in solids. *Computer Methods in Applied Mechanics and Engineering* 2011; **200**:649–664.
10. Prager W. Variational principles of linear elastostatics for discontinuous displacements, strains, and stresses. *Recent Progress in Applied Mechanics* 1967:463–474.
11. Virieux J. SH-wave propagation in heterogeneous media: Velocity-stress finite-difference method. *Geophysics* 1984; **49**:1933–1942.
12. Virieux J. P-SV wave propagation in heterogeneous media: Velocity-stress finite-difference method. *Geophysics* 1986; **51**:889–901.
13. Park KC, Lim SJ, Huh H. A method for computation of discontinuous wave propagation in heterogeneous solids: basic

algorithm description and application to one-dimensional problems. *International Journal for Numerical Methods in Engineering* 2012; **91**:622–643.
14. Cho SS, Park KC, Huh H. A method for multidimensional wave propagation analysis via component-wise partition of longitudinal and shear waves. *International Journal for Numerical Methods in Engineering* 2013; **95**:212–237.
15. Kolman R, Cho SS, Park KC. Efficient implementation of an explicit partitioned shear and longitudinal wave propagation algorithm. *International Journal for Numerical Methods in Engineering* 2016; **107**:543–579.
16. Gravouil A, Combescure A. Muti-time-step explicit-implicit method for non-linear structural dynamics. *International Journal for Numerical Methods in Engineering* 2001; **50**:199–225.
17. Gravouil A, Combescure A. Muti-time-step and two-scale domain decomposition method for non-linear structural dynamics. *International Journal for Numerical Methods in Engineering* 2003; **58**:1545–1569.
18. Gravouil A, Combescure A, Brun M. Heterogeneous asynchronous time integrators for computational structural dynamics. *International Journal for Numerical Methods in Engineering* 2015; **58**:1545–1569.
19. Park KC, Felippa CA. A variational framework for solution method developments in structural mechanics. *Journal of Applied Mechanics* 1998; **65**(1):242–249.
20. Park KC, Felippa CA. A variational principle for the formulation of partitioned structural systems. *International Journal for Numerical Methods in Engineering* 2000; **47**:395–418.
21. Park KC, Felippa CA, Gumaste UA. A localized version of the method of Lagrange multipliers and its applications. *Computational Mechanics* 2000; **24**(6):476–490.

APPENDIX

Multistep time integration in one-dimensional heterogeneous solids: In order to aid those interested in the present multistep integration algorithm, we offer a special case of one-dimensional problems below.

Fig. 29 shows two domains for one-dimensional heterogeneous problem. L-domain means a region with a larger time step, and S-domain is a region with a smaller time step. Γ_I is the internal interface between two domains, and $\mathbf{u}_f$ denotes the global displacement corresponding to the frame nodes in Γ_I. Two localized Lagrange multipliers, $\boldsymbol{\lambda}_L$ and $\boldsymbol{\lambda}_S$, are the internal interface loads at the corresponding frame nodes between two domains[21].

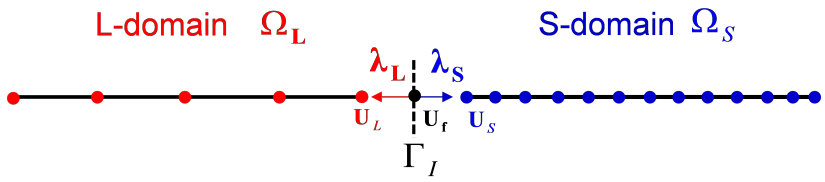

Figure 29. One dimensional heterogeneous solids including L-domain and S-domain.

Therefore, the equations of motion in two heterogeneous domains can be written as,

Equations of motion

$$\begin{aligned} \mathbf{M}_L\ddot{\mathbf{u}}_L + \mathbf{K}_L\mathbf{u}_L &= \mathbf{f}_L - \mathbf{B}_L\boldsymbol{\lambda}_L \; in \; \boldsymbol{\Omega}_L \\ \mathbf{M}_S\ddot{\mathbf{u}}_S + \mathbf{K}_S\mathbf{u}_S &= \mathbf{f}_S - \mathbf{B}_S\boldsymbol{\lambda}_S \; in \; \boldsymbol{\Omega}_S \end{aligned} \tag{37}$$

The subscripts, L and S, designate the larger time step domain and the smaller time step domain, respectively. $\mathbf{B}_L$ and $\mathbf{B}_S$ are the Boolean matrices that extracts the interface DOFs for each domains.

The accelerations and the interface loads at the interface DOFs should be continuous kinematically and kinetically as,

Kinematic interface continuities

$$\begin{aligned} \mathbf{B}_L^T\ddot{\mathbf{u}}_L - \mathbf{L}_L\ddot{\mathbf{u}}_f &= 0 \; on \; \Gamma_I \\ \mathbf{B}_S^T\ddot{\mathbf{u}}_S - \mathbf{L}_S\ddot{\mathbf{u}}_f &= 0 \; on \; \Gamma_I \end{aligned} \tag{38}$$

Traction continuities

$$\mathbf{L}_L^T\boldsymbol{\lambda}_L + \mathbf{L}_S^T\boldsymbol{\lambda}_S = 0 \; on \; \Gamma_I \tag{39}$$

where $\mathbf{L}_L$ and $\mathbf{L}_S$ are the Boolean matrices that relates the interface DOFs to the global acceleration

and displacement, and these are obtained by removing columns with all zero elements from $\mathbf{B}_L^T\mathbf{L}$ and $\mathbf{B}_S^T\mathbf{L}$, respectively. Equation (38)and Equation (39) satisfy all discontinuity conditions of displacement, strains and stresses at the interface between the heterogeneous domains[10]. The three continuity conditions is to obtain the Lagrange multipliers($\boldsymbol{\lambda}_L, \boldsymbol{\lambda}_S$ and $\mathbf{u}_f$) at the current integration time step. However, when two solids are perfectly bonded in highly heterogeneous materials, there is a possibility of 'the drifting' that the displacement and velocity at the corresponding interface can differ during the actual time integration. Therefore, the kinematic continuity conditions to prevent the drifting are applied to each integration step(t^{n+1}) of L-domain.

Kinematic continuities to prevent the drifting

$$\begin{aligned}\mathbf{B}_L^T\dot{\mathbf{u}}_L - \mathbf{L}_L\dot{\mathbf{u}}_f = \mathbf{B}_L^T\mathbf{u}_L - \mathbf{L}_L\mathbf{u}_f = 0 \; on \; \Gamma_I \\ \mathbf{B}_S^T\dot{\mathbf{u}}_S - \mathbf{L}_L\dot{\mathbf{u}}_f = \mathbf{B}_S^T\mathbf{u}_S - \mathbf{L}_S\mathbf{u}_f = 0 \; on \; \Gamma_I\end{aligned} \tag{40}$$

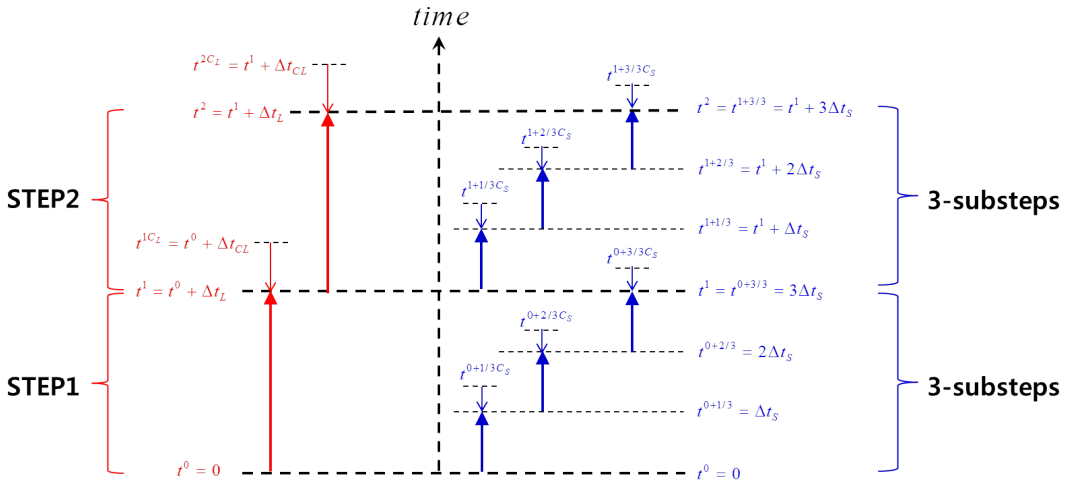

Figure 30. Procedures of multistep time integration for one dimensional heterogeneous solids.

Let's suppose that time step of large time step domain(L-domain) has 3 times lager than that of the small time step domain(S-domain) as shown in Fig. 30. In this case, during one time integration in the large time step domain, three time integration procedures should be separately done in small time step domain. Because we can skip two time integration procedures at L-domain in Fig. 30, we can reduce the total computing time.

The time step and the critical time step for L-domain are defined as follows.

$$\begin{aligned}Time\ at\ L-domain : t^{n+1} = t^n + \Delta t^{n+1} \\ Critical\ time\ step\ size : \Delta t_{CL} = L_{min}/C_L,\ C_L = \sqrt{E_L/\rho_L} \\ Integration\ time\ step\ size : \Delta t^{n+1} = \Delta t_L \\ Ratio\ of\ two\ time\ step\ sizes : \alpha_L = \Delta t_L/\Delta t_{CL}\end{aligned} \tag{41}$$

As in L-domain, the information of time step in S-domain can be written as:

$$\begin{aligned} Time\ at\ S-domain: t^{n+j} &= t^n + k\Delta t^{n+j} \\ Critical\ time\ step\ size: \Delta t_{CS} &= L_{min}/C_S,\ C_S = \sqrt{E_S/\rho_S} \\ Integration\ time\ step\ size: \Delta t^{n+j} &= \Delta t_S \\ Ratio\ of\ two\ time\ step\ sizes: \alpha_S &= \Delta t_S/\Delta t_{CS} \end{aligned} \tag{42}$$

where 'j' means the k-th integration sub-step in S-domain, and it is defined as follows.

$$\begin{aligned} j = \frac{k}{m} \le 1\ for\ k = 1, 2, \cdots, m \\ m = \Delta t_L/\Delta t_S \end{aligned} \tag{43}$$

where 'm' is the ratio of two time step sizes and is the integer, and 'k' is the order of sub-step in S-domain during a time step in L-domain. Therefore, we can state the displacement and acceleration of k-th substep of S-domain during (n+1)th step of L-domain as shown in Equation (44).

All elements on S(small step)-domain at $t^{n+j} = t^n + k\Delta t_S$

$$\begin{aligned} \mathbf{u}_S^{n+j} &= \mathbf{u}_S^{n+j_o} + \Delta t_S \dot{\mathbf{u}}_S^{n+j_o} + \beta_{1S}(\Delta t_{CS})^2 \ddot{\mathbf{u}}_S^{n+j_o} + \beta_{2S}(\Delta t_{CS})^2 \ddot{\mathbf{u}}_S^{n+jC_S} \\ \ddot{\mathbf{u}}_S^{n+j} &= \mathbf{M}_S^{-1}(\mathbf{f}_S - \mathbf{K}_S \mathbf{u}_S^{n+j}) - \mathbf{M}_S^{-1}\mathbf{B}_S \boldsymbol{\lambda}_S^{n+j} = \tilde{\ddot{\mathbf{u}}}_S^{n+j} - \mathbf{M}_S^{-1}\mathbf{B}_S \boldsymbol{\lambda}_S^{n+j} \\ \mathbf{u}_S^{n+jC_S} &= \mathbf{u}_S^{n+j_o} + \Delta t_{CS} \dot{\mathbf{u}}_S^{n+j_o} + \frac{1}{2}\Delta t_{CS}^2 \ddot{\mathbf{u}}_S^{n+j_o} \\ \ddot{\mathbf{u}}_S^{n+jC_S} &= \mathbf{M}_S^{-1}(\mathbf{f}_S - \mathbf{K}_S \mathbf{u}_S^{n+jC_S}) - \mathbf{M}_S^{-1}\mathbf{B}_S \boldsymbol{\lambda}_S^{n+jC_S} = \tilde{\ddot{\mathbf{u}}}_S^{n+jC_S} - \mathbf{M}_S^{-1}\mathbf{B}_S \boldsymbol{\lambda}_S^{n+jC_S} \\ \tilde{\ddot{\mathbf{u}}}_S^{n+j} &= \mathbf{M}_S^{-1}(\mathbf{f}_S^{n+j} - \mathbf{K}_S \mathbf{u}_S^{n+j}) \\ \tilde{\ddot{\mathbf{u}}}_S^{n+jC_S} &= \mathbf{M}_S^{-1}(\mathbf{f}_S^{n+jC_S} - \mathbf{K}_S \mathbf{u}_S^{n+jC_S}) \\ j_o &= \frac{k-1}{m}\ for\ k = 1, 2, \cdots, m \\ \alpha_S &= \Delta t_S/\Delta t_{CS} \\ \beta_{1S} &= \frac{\alpha_S}{6}(3\alpha_S + \theta - \theta\alpha_S^2) \\ \beta_{2S} &= \frac{\theta\alpha_S}{6}(\alpha_S^2 - 1) \end{aligned} \tag{44}$$

Unike the time integration of S-domain, L-domain does not require the k-th substep. Therefore, only (n+1)th integration step in L-domain is defined as shown in Equation (45).

All elements on L(large step)-domain at $t^{n+1} = t^n + m\Delta t_S$

$$\begin{aligned}
\mathbf{u}_L^{n+1} &= \mathbf{u}_L^n + \Delta t_L \dot{\mathbf{u}}_L^n + \beta_{1L}(\Delta t_{CL})^2 \ddot{\mathbf{u}}_L^n + \beta_{2L}(\Delta t_{CL})^2 \ddot{\mathbf{u}}_L^{n+C_L} \\
\ddot{\mathbf{u}}_L^{n+1} &= \mathbf{M}_L^{-1}(\mathbf{f}_L - \mathbf{K}_L \mathbf{u}_L^{n+1}) - \mathbf{M}_L^{-1}\mathbf{B}_L \boldsymbol{\lambda}_L^{n+j} = \tilde{\ddot{\mathbf{u}}}_L^{n+1} - \mathbf{M}_L^{-1}\mathbf{B}_L \boldsymbol{\lambda}_L^{n+1} \\
\mathbf{u}_S^{n+C_L} &= \mathbf{u}_L^n + \Delta t_{CL} \dot{\mathbf{u}}_L^n + \frac{1}{2}\Delta t_{CL}^2 \ddot{\mathbf{u}}_L^n \\
\ddot{\mathbf{u}}_L^{n+C_L} &= \mathbf{M}_L^{-1}(\mathbf{f}_L - \mathbf{K}_L \mathbf{u}_L^{n+C_L}) - \mathbf{M}_L^{-1}\mathbf{B}_L \boldsymbol{\lambda}_L^{n+C_L} = \tilde{\ddot{\mathbf{u}}}_L^{n+C_L} - \mathbf{M}_L^{-1}\mathbf{B}_L \boldsymbol{\lambda}_L^{n+C_L} \\
\tilde{\ddot{\mathbf{u}}}_L^{n+1} &= \mathbf{M}_L^{-1}(\mathbf{f}_L^{n+1} - \mathbf{K}_L \mathbf{u}_L^{n+1}) \\
\tilde{\ddot{\mathbf{u}}}_L^{n+C_L} &= \mathbf{M}_L^{-1}(\mathbf{f}_L^{n+C_L} - \mathbf{K}_L \mathbf{u}_L^{n+C_L}) \\
\alpha_L &= m\Delta t_S / \Delta t_{CL} = \Delta t_L / \Delta t_{CL} \\
\beta_{1L} &= \frac{\alpha_L}{6}(3\alpha_L + \theta - \theta\alpha_L^2) \\
\beta_{2L} &= \frac{\theta\alpha_L}{6}(\alpha_L^2 - 1)
\end{aligned} \tag{45}$$

However, the conditions that the displacement and the reaction force are continuous between L-domain and S-domain should be considered[10]. For this purpose, it is not necessary to consider all of the entire L-domain. Only 2-elements(E1 and E2) in L-domain next to the internal interface have only to satisfy the continuous conditions with S-domain for each substep because the internal forces of two nodes(N1 and N2) directly affect on the interface reaction force($\boldsymbol{\lambda}$) between two heterogeneous domains as shown in Fig. 31. The following equations (46) are k-th substep of 2-elements(E1 and E2) in L-domain next to the interface boundary.

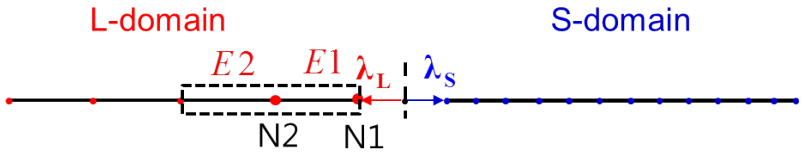

Figure 31. Two elements affecting on the interface loads $\boldsymbol{\lambda}_L$ and $\boldsymbol{\lambda}_S$.

Two elements(in L-domain) next to the interface at $t^{n+j} = t^n + k\Delta t_S$

$$\begin{aligned}
\mathbf{u}_L^{n+j} &= \mathbf{u}_L^n + k\Delta t_S \dot{\mathbf{u}}_L^n + \beta_{1L}(\Delta t_{CL})^2 \ddot{\mathbf{u}}_L^n + \beta_{2L}(\Delta t_{CL})^2 \ddot{\mathbf{u}}_L^{n+C_L} \\
\ddot{\mathbf{u}}_L^{n+j} &= \mathbf{M}_L^{-1}(\mathbf{f}_L - \mathbf{K}_L \mathbf{u}_L^{n+j}) - \mathbf{M}_L^{-1}\mathbf{B}_L \boldsymbol{\lambda}_L^{n+j} = \tilde{\ddot{\mathbf{u}}}_L^{n+j} - \mathbf{M}_L^{-1}\mathbf{B}_L \boldsymbol{\lambda}_L^{n+j} \\
\mathbf{u}_S^{n+C_L} &= \mathbf{u}_L^n + \Delta t_{CL} \dot{\mathbf{u}}_L^n + \frac{1}{2}\Delta t_{CL}^2 \ddot{\mathbf{u}}_L^n \\
\ddot{\mathbf{u}}_L^{n+C_L} &= \mathbf{M}_L^{-1}(\mathbf{f}_L - \mathbf{K}_L \mathbf{u}_L^{n+C_L}) - \mathbf{M}_L^{-1}\mathbf{B}_L \boldsymbol{\lambda}_L^{n+C_L} = \tilde{\ddot{\mathbf{u}}}_L^{n+C_L} - \mathbf{M}_L^{-1}\mathbf{B}_L \boldsymbol{\lambda}_L^{n+C_L} \\
\alpha_L &= k\Delta t_S / \Delta t_{CL}
\end{aligned} \tag{46}$$

All variables of two elements in L-domain at time $(t^{n+j} = t^n + k\Delta t_S)$ are calculated based on time steps (t^n) and $(t^n + \Delta t_{CL})$. Since the integration in L-domain is done only with two elements,

we can reduce the computing time. It is the most important thing of our present algorithm in terms of computing efficiency.

So far,we have described the integration variables of k-substep in S-domain, (n+1)-step in entire L-domain and k-substep of two elements in L-domain next to interface boundary, respectively. Since two heterogeneous domains have their own critical time step, the respective variables are integrated in domain-by-domain separately. However, the global acceleration, $\ddot{\mathbf{u}}_f$, and interface loads,$\boldsymbol{\lambda}_L$ and $\boldsymbol{\lambda}_S$, at the frame nodes in Γ_I are still unknown. The three unknown interface variables are able to be written from continuity conditions(Equation (38) and Equation (39)) and equations of motion(Equation (37)) at time t^{n+j} as shown in Equation (47).

$$\begin{bmatrix} \mathbf{B}_L^T\mathbf{M}_L^{-1}\mathbf{B}_L & 0 & \mathbf{L}_L \\ 0 & \mathbf{B}_S^T\mathbf{M}_S^{-1}\mathbf{B}_S & \mathbf{L}_S \\ \mathbf{L}_L^T & \mathbf{L}_S^T & 0 \end{bmatrix} \begin{bmatrix} \boldsymbol{\lambda}_L \\ \boldsymbol{\lambda}_S \\ \ddot{\mathbf{u}}_f \end{bmatrix}^{n+j} = \begin{bmatrix} \mathbf{B}_L^T\tilde{\ddot{\mathbf{u}}}_L^{n+j} \\ \mathbf{B}_S^T\tilde{\ddot{\mathbf{u}}}_S^{n+j} \\ 0 \end{bmatrix} \; for\ k = 1:m\ on\ \Gamma_I \tag{47}$$

The Equation (47) can be summarized as follows.

$$\begin{bmatrix} \boldsymbol{\lambda}_L \\ \ddot{\mathbf{u}}_f \end{bmatrix}^{n+j} = \begin{bmatrix} \mathbf{B}_L^T\mathbf{M}_L^{-1}\mathbf{B}_L & \mathbf{L}_L \\ \mathbf{L}_L^T & -\mathbf{L}_S^T(\mathbf{B}_S^T\mathbf{M}_S^{-1}\mathbf{B}_S)^{-1}\mathbf{L}_S \end{bmatrix}^{-1} \begin{bmatrix} \mathbf{B}_L^T\tilde{\ddot{\mathbf{u}}}_L^{n+j} \\ -\mathbf{L}_S^T(\mathbf{B}_S^T\mathbf{M}_S^{-1}\mathbf{B}_S)^{-1}\mathbf{B}_S^T\tilde{\ddot{\mathbf{u}}}_S^{n+j} \end{bmatrix}$$

$$\boldsymbol{\lambda}_S^{n+j} = (\mathbf{B}_S^T\mathbf{M}_S^{-1}\mathbf{B}_S)^{-1}[\mathbf{B}_S^T\tilde{\ddot{\mathbf{u}}}_S^{n+j} - \mathbf{L}_S\mathbf{u}_f^{n+j}] \tag{48}$$

As shown in Equation (48), we have to find the variables in the following order as shown in Equation (49).

$$\begin{aligned} \boldsymbol{\lambda}_S^{n+jC_S} &\rightarrow \ddot{\mathbf{u}}_S^{n+jC_S} \rightarrow \boldsymbol{\lambda}_S^{n+j} \\ \boldsymbol{\lambda}_L^{n+C_L} &\rightarrow \ddot{\mathbf{u}}_L^{n+C_L} \rightarrow \boldsymbol{\lambda}_L^{n+j} \end{aligned} \tag{49}$$

Therefore, $(\boldsymbol{\lambda}_S^{n+jC_S}, \boldsymbol{\lambda}_L^{n+C_L})$ should be obtained first in order to compute $(\boldsymbol{\lambda}_S^{n+j}, \boldsymbol{\lambda}_L^{n+j}, \ddot{\mathbf{u}}_f^{n+j})$, which are derived rigorously using basic equations shown in Fig. 32. Equations (50 ~ 52) show how to calculate the interface loads at their own critical time step.

Computation of $\boldsymbol{\lambda}^{n+jC_S}$ on Interface Γ_I of S-domain for $k = 1:m$

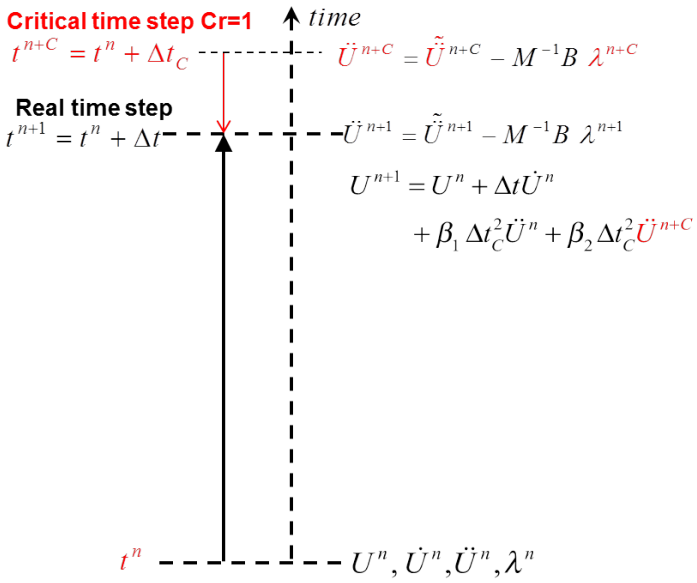

Figure 32. Procedures to get the interface load at the critical time step.

$$
\begin{aligned}
\Delta t &\triangleq \Delta t_{CS} \\
\mathbf{u}_S^{n+jC_S} &= \tilde{\mathbf{u}}_S^{n+jC_S} - \beta_{2S}(\Delta t_{CS})^2 \mathbf{M}_S^{-1}\mathbf{B}_S \boldsymbol{\lambda}_S^{n+jC_S} \\
\tilde{\mathbf{u}}_S^{n+jC_S} &= \mathbf{u}_S^{n+j_o} + \Delta t_{CS}\dot{\mathbf{u}}_S^{n+j_o} + \beta_{1S}(\Delta t_{CS})^2 \ddot{\mathbf{u}}_S^{n+(j_o} + \beta_{2S}(\Delta t_{CS})^2 \tilde{\ddot{\mathbf{u}}}_S^{n+jC_S} \\
\mathbf{u}_f^{n+jC_S} &= \mathbf{u}_f^{n+j_o} + \Delta t_{CS}\dot{\mathbf{u}}_f^{n+j_o} + \frac{1}{2}(\Delta t_{CS})^2 \ddot{\mathbf{u}}_f^{n+j_o} \\
\boldsymbol{\lambda}_S^{n+jC_S} &= [\beta_{2S}(\Delta t_{CS})^2 \mathbf{B}_S^T \mathbf{M}_S^{-1}\mathbf{B}_S]^{-1}(\mathbf{B}_S^T \tilde{\mathbf{u}}_S^{n+jC_S} - \mathbf{L}_S \mathbf{u}_f^{n+jC_S})
\end{aligned}
\tag{50}
$$

Computation of $\boldsymbol{\lambda}^{n+C_L}$ on Interface Γ_I of L-domain for $k = 1 : m$
(1) For k=1

$$
\begin{aligned}
\Delta t &\triangleq \Delta t_{CL} \\
\mathbf{u}_L^{n+C_L} &= \tilde{\mathbf{u}}_L^{n+C_L} - \beta_{2L}(\Delta t_{CL})^2 \mathbf{M}_L^{-1}\mathbf{B}_L \boldsymbol{\lambda}_L^{n+C_L} \\
\tilde{\mathbf{u}}_L^{n+C_L} &= \mathbf{u}_S^n + \Delta t_{CL}\dot{\mathbf{u}}_L^n + \beta_{1L}(\Delta t_{CL})^2 \ddot{\mathbf{u}}_L^{n)} + \beta_{2L}(\Delta t_{CL})^2 \tilde{\ddot{\mathbf{u}}}_L^{n+C_L} \\
\mathbf{u}_f^{n+C_L} &= \mathbf{u}_f^n + \Delta t_{CL}\dot{\mathbf{u}}_f^n + \frac{1}{2}(\Delta t_{CL})^2 \ddot{\mathbf{u}}_f^n \\
\boldsymbol{\lambda}_L^{n+C_L} &= [\beta_{2L}(\Delta t_{CL})^2 \mathbf{B}_L^T \mathbf{M}_L^{-1}\mathbf{B}_L]^{-1}(\mathbf{B}_L^T \tilde{\mathbf{u}}_L^{n+C_L} - \mathbf{L}_L \mathbf{u}_f^{n+C_L})
\end{aligned}
\tag{51}
$$

(2) For k=2:m

$$\begin{aligned}
\Delta t &\triangleq (k-1)\Delta t_S \\
\mathbf{u}_L^{n+C_L} &= \tilde{\mathbf{u}}_L^{n+C_L} - \beta_{2L}(\Delta t_{CL})^2 \mathbf{M}_L^{-1}\mathbf{B}_L \boldsymbol{\lambda}_L^{n+C_L} \\
\tilde{\mathbf{u}}_L^{n+C_L} &= \mathbf{u}_L^n + \Delta t_{CL}\dot{\mathbf{u}}_L^n + \beta_{1L}(\Delta t_{CL})^2 \ddot{\mathbf{u}}_L^{n)} + \beta_{2L}(\Delta t_{CL})^2 \tilde{\ddot{\mathbf{u}}}_L^{n+C_L} \\
\mathbf{L}_S \mathbf{u}_f^{n+j} &= \mathbf{B}_S^T \mathbf{u}_S^{n+j} \\
\boldsymbol{\lambda}_L^{n+C_L} &= [\beta_{2L}(\Delta t_{CL})^2 \mathbf{B}_L^T \mathbf{M}_L^{-1}\mathbf{B}_L]^{-1}(\mathbf{B}_L^T \tilde{\mathbf{u}}_L^{n+C_L} - \mathbf{L}_L \mathbf{u}_f^{n+C_L})
\end{aligned} \tag{52}$$

$\boldsymbol{\lambda}^{n+jC_S}$ is calculated explicitly in every substep as shown in Equation (50). And $\boldsymbol{\lambda}^{n+C_L}$ of interface Γ_I should be also updated in every substep as shown in Equation (51) and Equation (52) because ($\boldsymbol{\lambda}^{n+jC_S}$, $\mathbf{u}_f^{n+j}$) are recalculated in each substep.

There is also a alternative method for obtaining ($\boldsymbol{\lambda}_S^{n+jC_S}$ and $\boldsymbol{\lambda}_L^{n+C_L}$), which is to use a extrapolation by linear convex combination as following Equations (53, 54) as a similar way with reference [18].

Alternative method of computing $\boldsymbol{\lambda}_S^{n+jC_S}$ on S-domain

$$\begin{aligned}
\alpha_S &= \Delta t_S / \Delta t_{CS} \\
\boldsymbol{\lambda}_S^{n+j} &= (1-\alpha_S)\boldsymbol{\lambda}_S^{n+j_0} + \alpha_S \boldsymbol{\lambda}_S^{n+jC_S}
\end{aligned} \tag{53}$$

Alternative method of computing $\boldsymbol{\lambda}_L^{n+C_L}$ on L-domain

$$\begin{aligned}
\alpha_L &= k\Delta t_S / \Delta t_{CL} \\
\boldsymbol{\lambda}_L^{n+j} &= (1-\alpha_L)\boldsymbol{\lambda}_L^{n} + \alpha_L \boldsymbol{\lambda}_L^{n+C_L}
\end{aligned} \tag{54}$$

However, our numerical experiment using the alternative method showed that $\boldsymbol{\lambda}_S^{n+j} \neq \boldsymbol{\lambda}_L^{n+j}$ in case of $\Delta t_{CL} >> \Delta t_{CS}$. So, we did not adopted the alternative method for obtaining more accurate solution in the present algorithm. Despite our present is shown as more or less complicated, the present algorithm has the advantage that the calculation time is drastically reduced since L-domain is computed only in two elements next to the internal interface at each substep, and that the solution is more accurate specially in case of $\Delta t_{CL} >> \Delta t_{CS}$

Now we state a step-by-step present algorithm for one dimensional heterogeneous solids.

Flowchart of multistep time integration for two-dimensional heterogeneous solids

Start of Main Step $n = 1 : N$ on L-domain

Step 1 : Prepare $(\mathbf{u}_L^n, \dot{\mathbf{u}}_L^n, \ddot{\mathbf{u}}_L^n)$

Start of Substep $k = 1 : m$ on S-Domain

Step 2 : Prepare $(\mathbf{u}_S^{n+j_o}, \dot{\mathbf{u}}_S^{n+j_o}, \ddot{\mathbf{u}}_S^{n+j_o})$
Step 2.1 : Compute $(\boldsymbol{\lambda}_S^{n+j}, \boldsymbol{\lambda}_L^{n+j}\ and\ \ddot{\mathbf{u}}_f^{n+j})$ at the interface, Γ_I
Step 2.1.1 : Compute $(\boldsymbol{\lambda}_S^{n+jC_S})$
Step 2.1.2 : Compute $(\boldsymbol{\lambda}_L^{n+C_L})$
Step 2.1.3 : Compute $(\boldsymbol{\lambda}_S^{n+j}, \boldsymbol{\lambda}_L^{n+j}\ and\ \ddot{\mathbf{u}}_f^{n+j})$
Step 2.2 : Compute $(\dot{\mathbf{u}}_S^{n+j}, \ddot{\mathbf{u}}_S^{n+j)})$

$$\begin{aligned} \ddot{\mathbf{u}}_S^{n+j} &= \tilde{\ddot{\mathbf{u}}}_S^{n+j} - \mathbf{M}_S^{-1}\mathbf{B}_S\boldsymbol{\lambda}_S^{n+j} \\ \dot{\mathbf{u}}_S^{n+j} &= \dot{\mathbf{u}}_S^{n+(j-1)} + \Delta t_S\{(1-\gamma)\ddot{\mathbf{u}}_S^{n+(j-1)} + \gamma\ddot{\mathbf{u}}_S^{n+j}\} \end{aligned} \tag{55}$$

Step 2.3 : Update $(\mathbf{u}_f^{n+j}, \dot{\mathbf{u}}_f^{n+j)})$ at the interface, Γ_I

$$\begin{aligned} \dot{\mathbf{u}}_f^{n+j} &= \dot{\mathbf{u}}_f^{n+(j-1)} + \Delta t_S\{(1-\gamma)\ddot{\mathbf{u}}_f^{n+(j-1)} + \gamma\ddot{\mathbf{u}}_f^{n+j}\} \\ \mathbf{u}_f^{n+j} &= \mathbf{u}_f^{n+(j-1)} + \Delta t_S\dot{\mathbf{u}}_f^{n+j} \end{aligned} \tag{56}$$

END of Substep on S-Domain

Step 3 : Compute $(\dot{\mathbf{u}}_L^{n+1}, \ddot{\mathbf{u}}_L^{n+1)})$ on entire L-domain
Step 3.1 : Compute $(\dot{\mathbf{u}}_L^{n+1}, \ddot{\mathbf{u}}_L^{n+1)})$

$$\begin{aligned} \ddot{\mathbf{u}}_L^{n+1} &= \tilde{\ddot{\mathbf{u}}}_L^{n+1} - \mathbf{M}_L^{-1}\mathbf{B}_L\boldsymbol{\lambda}_L^{n+1} \\ \dot{\mathbf{u}}_L^{n+1} &= \dot{\mathbf{u}}_L^{n} + \Delta t_L\{(1-\gamma)\ddot{\mathbf{u}}_L^{n} + \gamma\ddot{\mathbf{u}}_L^{n+1}\} \end{aligned} \tag{57}$$

Step 3.2 : Update $(\mathbf{u}_L^{n+1}, \dot{\mathbf{u}}_L^{n+1)})$ only at the interface, Γ_I, to prevent the drifting of the interface

$$\begin{aligned} \mathbf{L}_L\mathbf{u}_L^{n+1} &= \mathbf{B}_L^T\mathbf{u}_f^{n+1} \\ \mathbf{L}_L\dot{\mathbf{u}}_L^{n+1} &= \mathbf{B}_L^T\dot{\mathbf{u}}_f^{n+1} \end{aligned} \tag{58}$$

END of Main Step on L-domain